東京大学 大学院新領域創成科学研究科
基盤科学研究系
先端エネルギー工学専攻

平成 19 年度

修士論文

Synthesis of Carbon Films with Applying Negative DC Bias Voltages in Surface Wave excited Plasma CVD Apparatus

－　表面波プロセスプラズマを用いた負の直流バイアス電圧印加によるカーボン系薄膜合成　－

2008 年 2 月提出
指導教員　大崎　博之　教授

66208　キム　ドンミン

1. Introduction

1.1. Process plasma and plasma sources

Plasma processing is one of the most important technologies in the modern industry such as aerospace, automotive, biomedical, and environmental. Especially, plasma based processes for surface modification are essential for manufacturing the very large scale integrated circuits (ICs) used by the electronics industry. Some properties of surface that could be modified with superficial treatment of materials using plasma are shown in table 1.1.1. Moreover, it is possible to synthesize unique materials such as diamond films, diamond-like carbon (DLC) films, and amorphous silicon for solar cells [l].

Table 1.1.1 Plasma based treatment for surface modification of material [2]

Surface properties that could be modified	Application field
Generation of low friction surfaces	Biomedical (tools for endoscopy)
Improvement of biocompatibility	Biomedical (orthopaedic prothesis)
Increase of corrosion resistance	Mechanical
Increase of wear resistance	Mechanical (cutting tools)
Increase of scratch resistance	Optic (lens fro glasses, contact lens)
Increase of depth of dyeing	Textile industry
Decrease of wetting	Textile industry
Decrease of fluids permeability	Food packaging industry
Aesthetical and functional increase	Decorative components industry
Increase of wetting	Paper industry

As plasma based processes have become essential to the modern industry, followed things have been considered as the most important issues in the development of plasma sources [3-4].

- High radical density for high productivity
- Uniform plasma density for a large area process
- Low-pressure plasma for a subtle process

In order to fulfill these industrial demands, various plasma sources have been developed and studied. Recently, plasmas that are discharging and sustaining by electromagnetic waves of 13.56 MHz radio frequency (RF) or 2.45 GHz microwave have widely used and applied at the industrial process. Plasma devices with RF sources, such as helicon plasma, helical resonator plasma, and inductively coupled plasma (ICP), are shown in figure 1.1.1. These RF plasma devices have several advances as follows.

- It is possible to produce large-area plasmas with uniform density.
- Discharging is very stable comparing with DC discharging method.

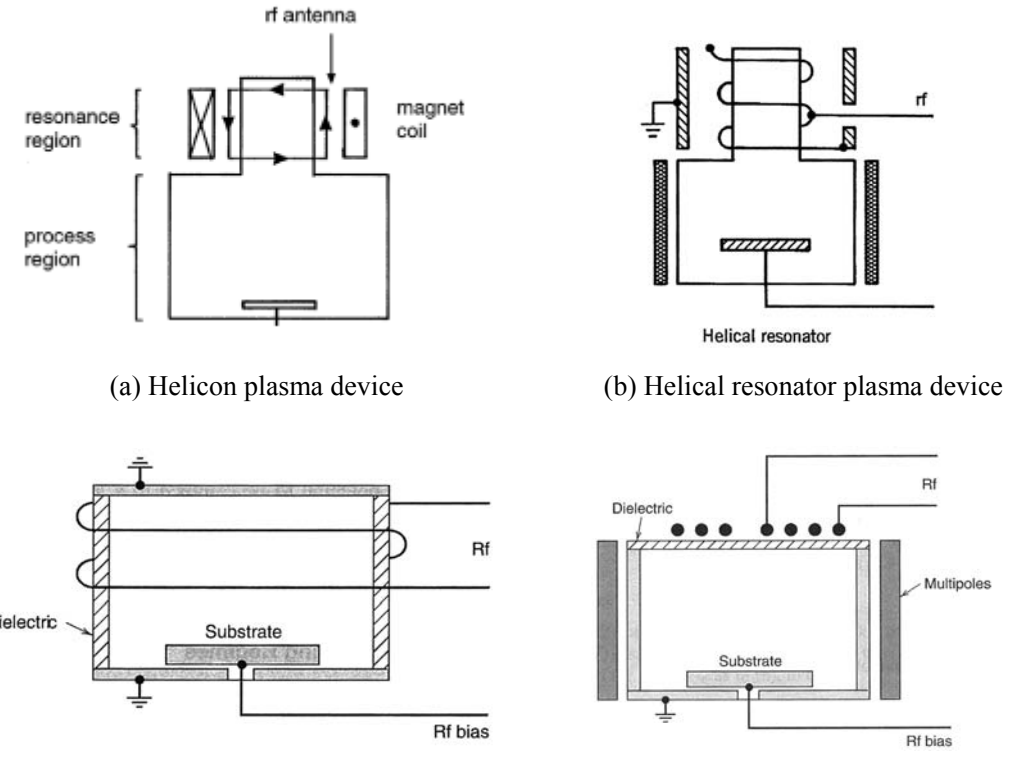

(a) Helicon plasma device (b) Helical resonator plasma device

(c) ICO device (d) ICP device in planar geometry

Figure 1.1.1 Schematic illustrations of RF plasma devices [1]

Whereas, microwave plasmas have some more advantages compared with RF plasmas as follows [5].

- Any electrodes are not needed that is prevented contamination from electrodes.
- Discharging can be maintained stable at wide range of gas pressure.
- Because incident microwave travels along wave-guide, radiation loss is small and impedance matching is possible with the use of simple components.

However, some defects on microwave plasmas have been indicated as follows.

- The incident microwaves are reflected at the plasma interface having a higher density than the cut-off density (i.e. 7.4×10^{10} cm^{-3} at 2.45 GHz).
- The generating area is limited from the size of wave-guide

Because of theses disadvantages, generating plasmas with a high density and a large-area using microwave has been difficult. However, the developments of electron cyclotron resonance (ECR) plasmas device and surface wave exited plasma (SWP) device make to overcome these disadvantages.

An ECR plasmas source is shown in figure 1.1.2. One or more electromagnet coils placed at the cylindrical source chamber generate an axially varying magnet field. Microwave is injected axially into the source chamber and excites a right circularly polarized wave propagates along the dc magnetic field lines to a resonance zone, where the wave energy is absorbed.

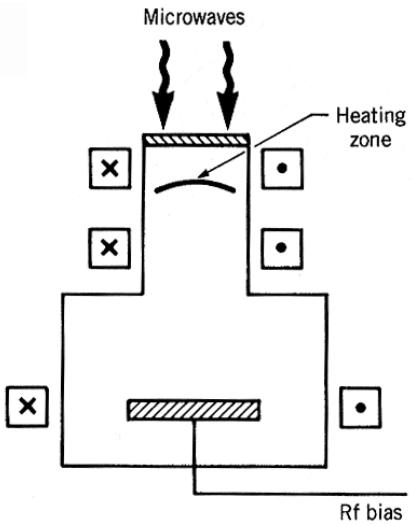

Figure 1.1.2 Schematic illustrations of electron cyclotron resonance (ECR) plasma [1]

On the other side, SWP devices generate high and uniform density plasmas over a large area without applying any external magnetic field. An electromagnetic wave launched along the surface of plasma propagates and sustained SWPs. The details about SWPs are presented in chapter 1.2.

1.2. Surface Wave exited Plasma (SWP)

The surface wave (SW) is a wave bounded by the interface between two systems. For examples, the ripple phenomenon in water is a surface wave guided by the interface between air and water [6]. In electromagnetics, SW is an electromagnetic wave that propagates along the interface of dielectric and lossy conductor. And the wave in this propagation mode has a feature, which the electromagnetic field is attenuated exponentially with being off perpendicularly from the dielectric, as shown in figure 1.2.1.

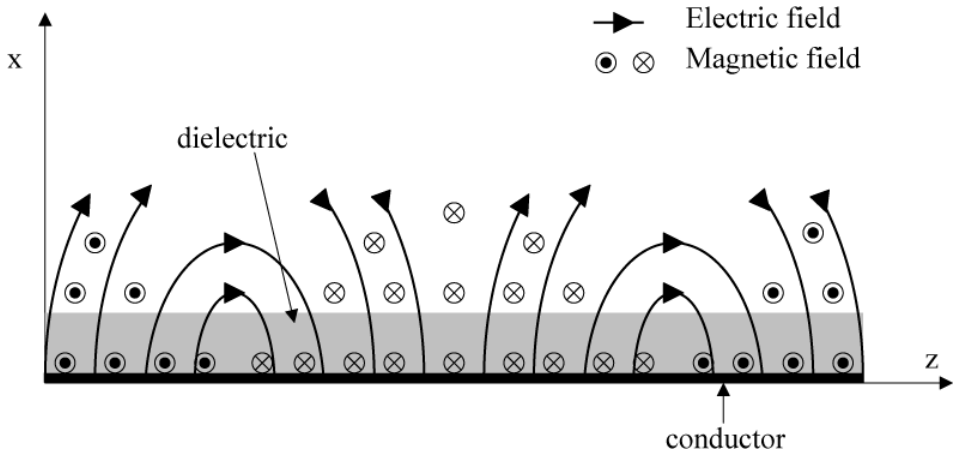

Figure 1.2.1 Schematics of surface wave propagation with TM mode [7]

1.2.1. Surface waves in wave guided with plasmas

SWs, which are propagating waves having strong fields only near the plasma surface, can be efficiently absorbed by the plasma, and sustaining a discharge. Since the end of the 1950s, discharges that are excited and sustained by surface waves, which are propagating along the dielectric-plasma interface, have been studied [8]. Moisan's group have widely analyzed the concept and studied about various types of the wave launchers [9-11]. And various configurations of the waveguiding systems have also been studied by several groups [12-15]. Cylindrical surface wave sources have been reviewed by Moisan and Zakrewski in 1991 [16]. Hence, the cylindrical configuration cannot be operated as a low aspect ratio source. However, planar (rectangular) configurations have been developed (Komachi, 1993) that may be suitable for large-area processing applications [17].

At the beginning of the 1980s, the linear approach to wave propagation in homogenous plasma wave-guides was clearly understood. However, the growing activity on discharges produced by propagating surface waves and on nonlinear surface waves creates the necessity for additional investigations of the dispersion behavior of the waves.

The main defining features of surface waves in wave-guided with homogenous plasmas are as follows [18]:

- The surface waves are proper modes of bounded systems
- They propagate along interfaces between two media different permittivities.
- The wave field amplitudes - which have maximum values at the interface - decrease with distance from the interface into the two media.

1.2.2. Electromagnetic waves and plasma oscillations in an infinite plasma [18-22]

Assuming that thermal motions and particle collisions can be neglected, the dispersion equation of an electromagnetic wave that propagates with a frequency of $f = \omega/2\pi$ in an infinite homogenous non-magnetized plasma is

$$\omega^2 = \omega_p^2 + c^2\mathbf{k}^2, \tag{1.1}$$

where **k** is the wave vector, c is the speed of light in free space, and ω_p is the electron plasma frequency.

The electron plasma frequency is described by

$$\omega_p = e\left(\frac{n_e}{\varepsilon_0 m_e}\right)^{\frac{1}{2}} \tag{1.2}$$

with electron density n_e, electron mass m_e, elementary charge e, and permittivity of free space ε_0.

The phase velocity v_{ph} is given by

$$v_{ph} = \frac{c}{\sqrt{\varepsilon_p}} = \frac{\omega}{k}, \tag{1.3}$$

where a plasma permittivity ε_p.

Introducing this equation into the equation (1.1), we can obtain

$$\varepsilon_p = 1 - \left(\frac{\omega_p}{\omega} \right)^2 . \tag{1.4}$$

Applying the electron-neutral collision frequency with momentum transfer ν to this equation, then the plasma permittivity is given by

$$\varepsilon_p = 1 - \frac{\omega^2}{\omega(\omega + i\nu)} . \tag{1.5}$$

The cut-off plasma density can be modified with introducing the electron plasma frequency as wave frequency, when the plasma permittivity become zero. Thus, the cut-off plasma density n_c is given by

$$n_c = \frac{\varepsilon_0 m_e \omega^2}{e^2} . \tag{1.6}$$

For example, if the wave frequency is 2.45 GHz, the critical cut-off density is $n_c = 7.4 \times 10^{10}$ cm^{-3}.

In the case of infinite plasmas, electromagnetic waves can propagate over longer distance with relatively low attenuation only at underdense conditions (i.e. $n_e < n_c, 0 < \varepsilon_p < 1$).

In overdense conditions (i.e. $n_e > n_c, \varepsilon_p < 0$), electromagnetic waves are evanescent and decay exponentially. And the skin depth derived from the dispersion equation (1.1) is given by

$$\delta = \frac{1}{|\mathrm{Im}\, k|} = \frac{c}{\sqrt{\omega_p^2 - \omega^2}} . \tag{1.7}$$

Thus, in case of plasmas with high density, the skin depth is given by

$$\delta = \frac{c}{\omega_p} . \tag{1.8}$$

1.2.3. Electromagnetic waves in bounded plasma [20]

In real bounded plasma, electromagnetic waves propagate with features as follows.

- In underdense plasma bounded condition, the electromagnetic waves penetrate into plasma as volume wave (figure 1.2.2 (a)).
- In overdense plasma bounded condition, the electromagnetic waves cannot penetrate into plasma, but an surface wave can propagate along the dielectric-plasma interface, and penetrate into the plasma at a few of the skin depth (figure 1.2.2 (b)).

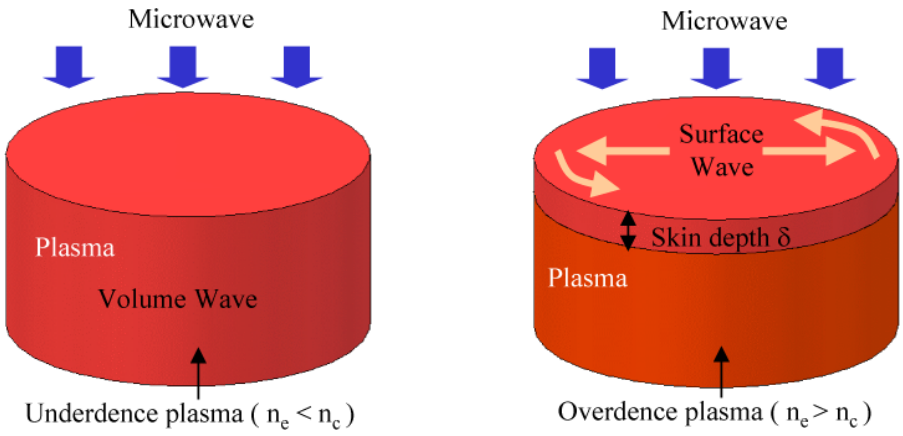

(a) Uunderdense plasma (b) Overdence plasma

Figure 1.2.2 Electromagnetic wave propagation in finite plasmas

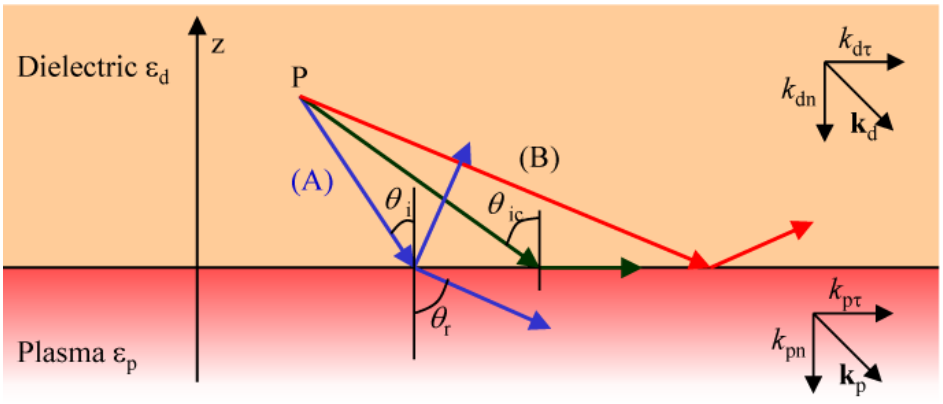

Figure 1.2.3 Electromagnetic wave propagation along plasma-dielectric interface

Assuming an electromagnetic wave propagates along the plane interface between a semi-infinite dielectric of permittivity ε_d and a semi-infinite plasma as shown in figure 1.2.3.

The wave vector component parallel to the normal direction of the surface in the plasma and in the dielectric is given by

$$k_{pn} = \sqrt{\frac{\varepsilon_p \omega^2}{c^2 - k_{p\tau}^2}} = \sqrt{\frac{\left(\omega^2 - \omega_P^2\right)}{c^2 - k_{p\tau}^2}} \tag{1.9}$$

and

$$k_{dn} = \sqrt{\frac{\varepsilon_d \omega^2}{c^2 - k_{d\tau}^2}}, \tag{1.10}$$

where k_{dn} and $k_{d\tau}$ are the wave vector components of normal and tangential to the interface in the dielectric and k_{pn} and $k_{p\tau}$ are the wave vector components of normal and tangential to the interface in the plasma, respectively.

The boundary conditions along the plasma-dielectric interface require $k_{d\tau} = k_{p\tau}$, thus it is possible to denote them simply as k_τ:

$$k_{d\tau} = k_{p\tau} = k_\tau \tag{1.11}$$

In figure 1.2.3, some examples of rays of electromagnetic waves injected from any point P in dielectric region into the plasma are shown. Assuming that ε_d and ε_p are real and, the incidence and reflection angles with respect to the surface normal are

$$\theta_i = \tan^{-1}\left(\frac{k_\tau}{k_{dn}}\right) \tag{1.12}$$

and

$$\theta_r = \tan^{-1}\left(\frac{k_\tau}{k_{pn}}\right) \tag{1.13}$$

respectively.

As it is well known in geometrical optics that the ray trajectory follows Snell's law, we can obtain

$$\left(\frac{\varepsilon_p}{\varepsilon_d}\right)^{\frac{1}{2}} = \frac{\sin\theta_i}{\sin\theta_r}, \tag{1.14}$$

from equations of (1-9)~(1-14). And in case that the ray reflected totally along the interface (i.e. $\theta_r = \pi/2$), the critical incidence angle is given by

$$\theta_{ic} = \sin^{-1}\left(\sqrt{\frac{\varepsilon_p}{\varepsilon_d}}\right) \tag{1.15}$$

As shown in figure 1.2.3, the ray trajectories could be classified into two groups depending on the incidence angle θ_i as follows.

(A) In case of $\theta_i < \theta_{ic}$, the volume wave penetrates into the plasma bulk

(B) In case of $\theta_i > \theta_{ic}$, the volume wave reflected at the interface of dielectric and plasma, and the amplitude of the latter decrease exponentially from the interface into the plasma.

But if the plasma is in overdense condition, the plasma permittivity ε_p becomes negative and the volume waves cannot penetrate into the plasma. In this case, a new type of electromagnetic wave is generated. The amplitude decays exponentially from the interface into both directions of the dielectric and the plasma as shown in figure 1.2.4 (C). These waves are usually referred to as surface waves.

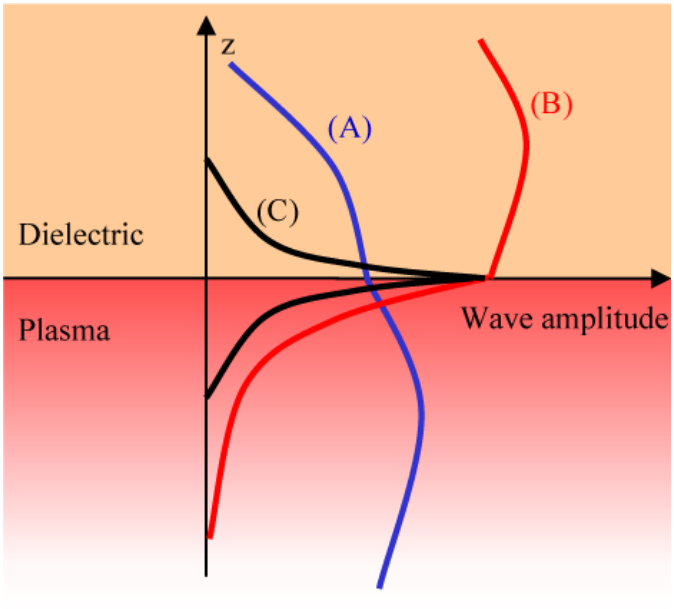

Figure 1.2.4 Wave field distribution on both sides of the dielectric-plasma interface for volume waves

1.2.4. Surface wave exited plasma apparatus for a large-area process

In the end of the 1980s, Komachi *et al*. have developed a large-area SWP device with a planar configuration of rectangular dielectric waveguide. However, there are some problems that the discharge tends to be spatially localized, and that affects the matching condition significantly. Due to very small changes in discharge conditions, unstable plasma is resulted. This problem has been overcome by developing a new configuration of wave guiding structure with slot antennas.

The slot antenna system developed by Werner *et al*. [23] contained an annular waveguide resonator with axial slots at the inner side, and sustained plasmas in the discharging chamber using incident microwaves of 2.45 GHz frequency.

Nagatsu *et al*. [24] developed a large-diameter plasma apparatus discharged and sustained by 2.45 GHz microwaves through a pair of inclined slot antennas. The chamber consisted of two sections, and the upper section was for discharging and sustaining plasma and the lower section was for reacting.

Kanoh *et al*. [25] investigated the optimal shape of the slot antenna for generating uniform plasmas by adjusting the angle of the slot antenna. And the plasma could be generated in the direction perpendicular to the axis of the slot antenna.

In this study, a ring dielectric line typed surface wave plasma (RDL-SWP) apparatus, which was developed by Sumitomo Metal Industries, is used. This apparatus has an antenna part consisted of a ring typed dielectric and 16 slots under that. The details about this apparatus are explained in chapter 3.

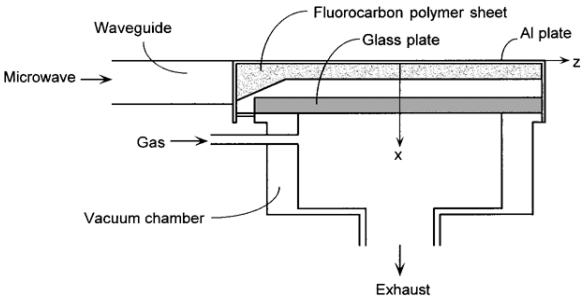

(a) by Komachi et al. [26]

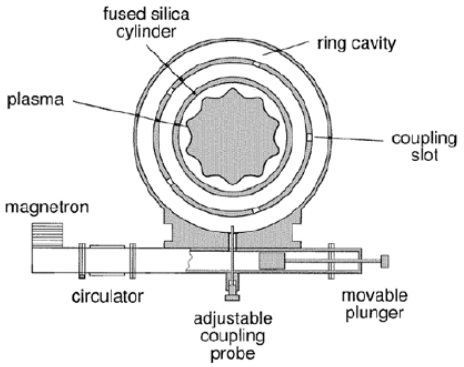

(b) by Werner at al. [23]

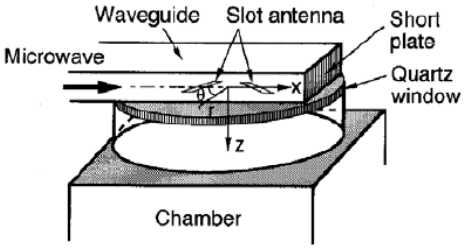

(c) by Nagatsu et al. [24]

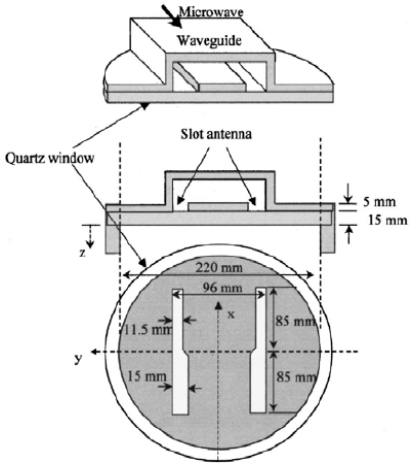

(e) by Kabnoh et al [25]

Figure 1.2.5 Planar type SWP process devices

1.3. Carbon films synthesized by Plasma enhanced Chemical Vapor Deposition

1.3.1. Carbon materials and diamond films

Carbon materials such as diamond-like carbon (DLC) films, chemical vapor deposition (CVD) diamond films, nanotube have been advanced enormously with the development of plasma technologies. And these carbon materials are indispensable in various modern industrial fields such as mechanical, biomedical, chemical, and MEMS/NEMS [27].

Carbon films synthesized by Plasma CVD usually can be classified into CVD diamond film and DLC film consists of tetrahedral carbon (ta-C) and amorphous diamond (a-D) with concentration of sp^2 and sp^3 carbon structures (shown in figure 1.3.1) in that. A significant amount of sp^3 carbon structure in the films gives them attractive physical and mechanical properties such as high hardness, high wear resistance, low coefficient of friction, chemical inertness, a high optical band-gap, and high electrical resistivity. The hydrogenated amorphous carbon (a-C:H) film is also designated as DLC film. Classification diagram of carbon films is shown in figure 1.3.2.

The CVD diamond film has been synthesized in the early of the 1980s by Matumoto *et al*. They synthesized diamond films at gas pressure of 10~100 Torr and substrate temperature of 700~1000℃. Since that study, many studies have been carried out for investigating mechanism of the diamond films deposition, and various deposition systems have been developed. Recently, plasma enhanced CVD method is most widely used on synthesizing diamond films [28]. Because these CVD diamond films have enormous potential utility in various fields, many applications such as tool and seal coatings, optical windows, surface acoustic wave (SAW) devices, electrochemical electrodes, conformal coatings for microelectromechanical systems (MEMS) or nano-electromechanical system, and electron-emitting surfaces for flat-panel displays have been studied [29-31].

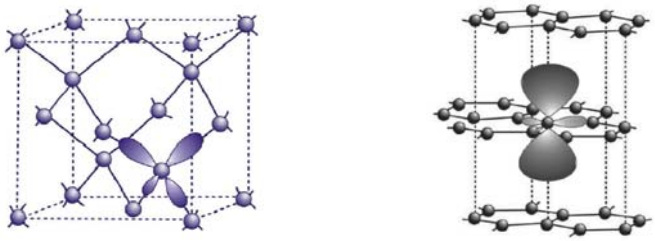

(a) sp3 Diamond structure (b) sp2 Graphite structure

Figure 1.3.1 Schematics illustration of carbon structure

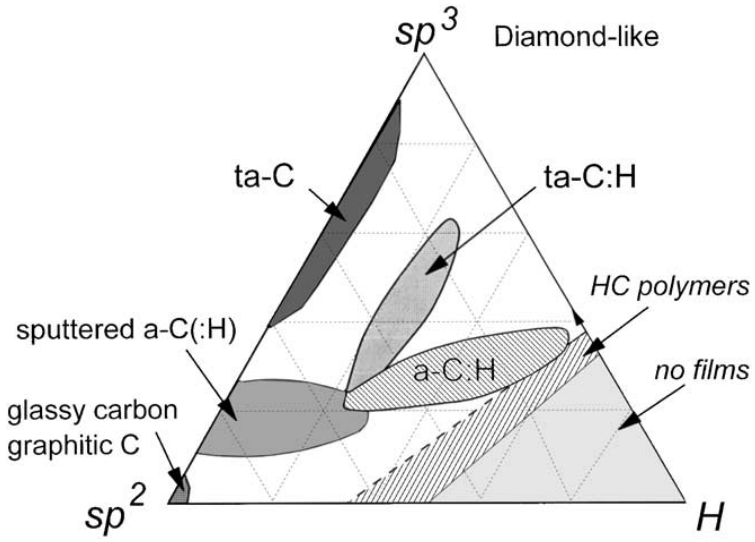

Figure 1.3.2 Ternary phase diagram of bonding in amorphous carbon-hydrogen alloys [27]

1.3.2. Mechanism of carbon material deposition in plasma CVD

In plasma enhanced CVD system, various parameters influence on carbon material depositions as shown in figure 1.3.3. These parameters are linked each other's, and that makes it very difficult to analysis the substantial mechanism of carbon material deposition. However, it is very clear that controlling the sp^3 concentration is a very important issue for controlling the properties of deposited carbon material.

Usually, hydrogen based gas mixtures with carbon containing gas species are used as source gases in synthesizing carbon films by plasma CVD. That reason is why the atomic hydrogen performs key roles in CVD process to obtain high concentration of sp^3 carbon structure. The roles of atomic hydrogen are as follows [21].

- Preferential etching of graphite over diamond: the removal of graphite by activated hydrogen is orders of magnitude faster than for diamond.
- Stabilization of the diamond surface by satisfying the dangling bonds of surface carbons, maintaining these carbons in an sp^3 configuration and preventing surface reconstruction into graphitic sp^2 or carbynic sp structures.
- Removal of hydrogen from surface C_d-H bonds to create active growth sites, and removal of H from the growth surface to avoid trapping of hydrogen in the solid, as occurs with amorphous hard carbons. C_d represents carbon on a diamond surface.
- Promotion of gas-phase production of growth precursors, as well as the sp^3 configuration of gaseous radical precursors and surface clusters.
- Removal of oxygen chemisorbed onto the substrate.

Various radicals are generated in discharging chamber from injected source gas by plasma as shown in figure 1.3.3. Therefore, hydrocarbon free radicals such as CH3, CH2, and CH deposit not only diamond contents but also graphitic contents on the inserted substrate. However, the atomic hydrogen radicals produced simultaneously by plasma etch the graphitic contents and non-diamond components as explained above. Moreover, in oxygen mixture gas phase (i.e. C-H-O mixture system), the radicals containing oxygen such as OH, OH+ is known to improve the etching ability for the non-diamond contents. For that reason, diamond films depositions are possible although at the condition of a very low substrate temperature of ~350℃ [28].

These deposition processes are affected by various deposition parameters such as plasma parameter, gas pressure, substrate temperature, and gas mixture concentration. Besides, the ion bombardment is also a very important parameter that has to control, to obtain high concentration of sp^3 carbon structure of them, because the ion bombardment into the substrate enhances the nucleation for diamond growth but also formation non-diamond contents or lattice disordering on it.

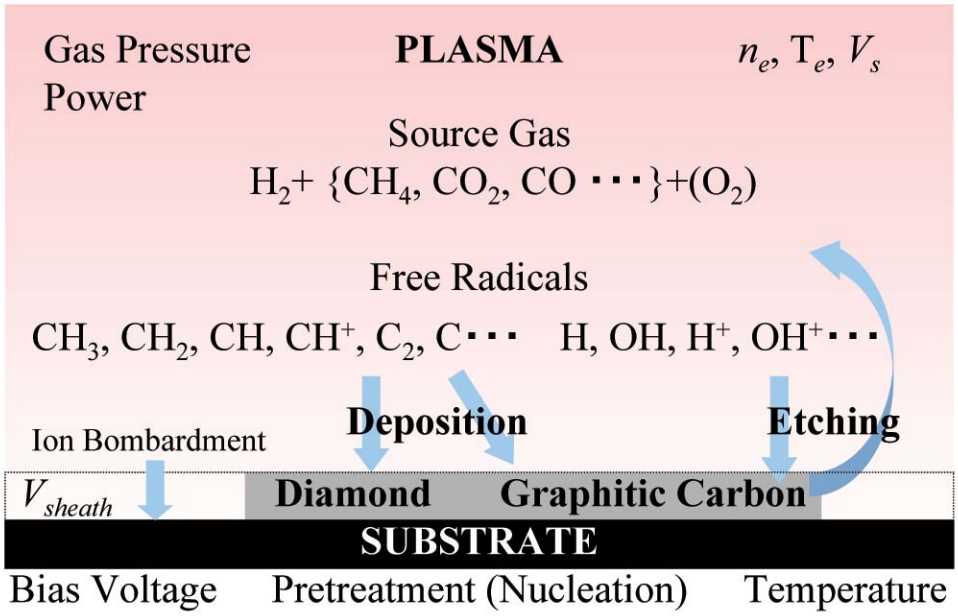

Figure 1.3.3 Schematic illustration of mechanism of diamond film deposition

1.3.3. Deposition process at a low gas pressure

At low pressure, the deposition process is highly influenced by synergistic effects of energetic ions on chemical reactions of radicals at the surface. Teii *et al*. have investigated the factors being responsible for the pressure limit as follows [32,33].

- High ion energy
- Low radical density
- High ion-to-neutral (adatom) flux ratio

To control the high ion bombardment into the substrate, DC or RF bias voltages usually are applied to the metallic substrate holder. Applying positive bias voltage decreases the sheath potential on substrate, and the ion energy into the substrate is decreased. However, a problem that the plasma potential is increased simultaneously and that results in unstable plasma has been reported in these bias methods. Moreover, in RDL-SWP plasma, it has been reported that applying positive DC bias voltage generates an arc-like discharging at the condition of bias voltages over 50V.

To overcome this bias limitation, J. Kim *et al*. [21,34] developed a new typed bias method and succeed to synthesize a high quality nanocrystalline diamond films with continuous layers. The main concept of this new bias method is controlling the plasma space potential of reacting region to decrease the ion bombardment energy into the substrate. The details of this bias method are presented in chapter 2.

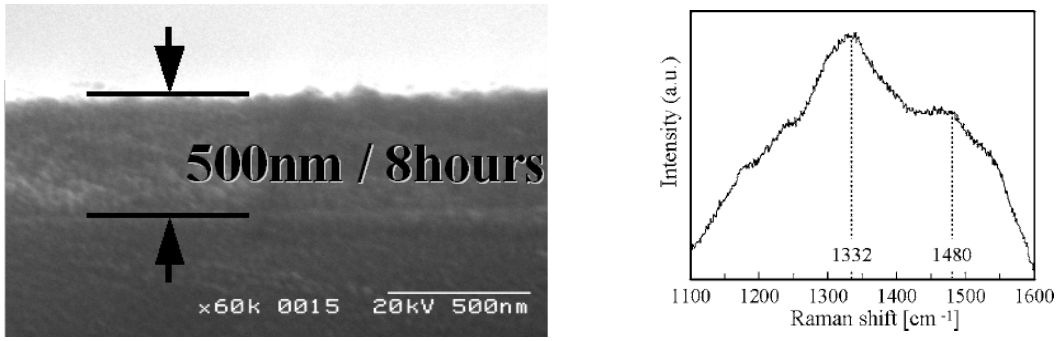

(a) SEM image of NCD films (b) Raman spectra

Figure 1.3.4 NCD film deposited by J. Kim in RDL-SWP apparatus [21,34]

1.4. Previous experiments for carbon material depositions

In previous experiments, a NCD film was synthesized in RDL-SWP apparatus at a low gas pressure of 30 mTorr and low substrate temperature of ~430℃, using the new DC bias method developed by J. Kim. The experimental details and results are presented in the following section.

1.4.1. Experimental setup

The experimental setup is shown in figure 1.4.1. The RDL-SWP apparatus was basically constructed as same to the one of high quality NCD film deposited experiment. An n-type mirror-polished silicon (100) was used as a substrate. The substrate was just cleaned in methanol without any pre-treatment for the nucleation of diamond, and placed on the substrate holder grounded electrically. The mixture gas of 98%H2-3%CO was injected to the discharging chamber as source gas and the gas pressure was 30 mTorr. Carbon films were deposited under the conditions of deferent bias voltages from –100V to –190V and the substrate temperatures was heated to ~430℃ only by plasma. The incident microwave power was 1.5 kW. The deposited films were investigated by Raman spectroscopy and X-ray diffraction.

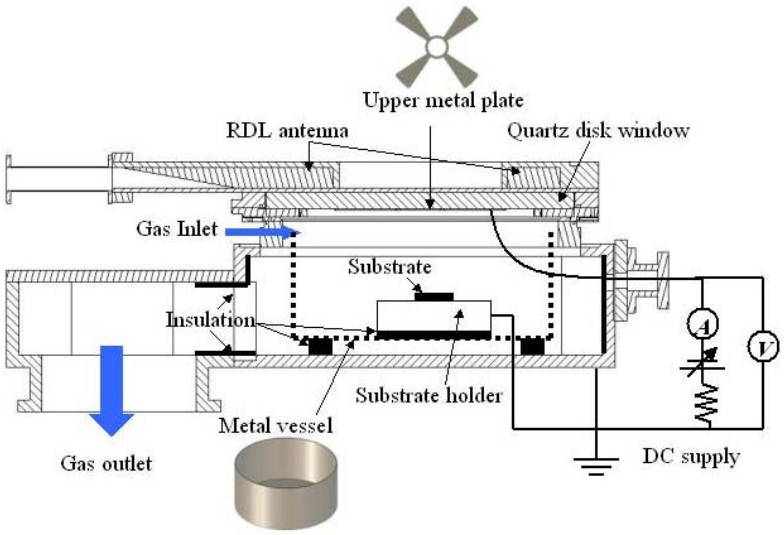

Figure 1.4.1 Schematic illustration of experimental setup

1.4.2. Film measurement results and discussions

Raman spectra and XRD patterns of the deposited films are shown in figure 1.4.2 and figure 1.4.3. In case of natural diamond, the Raman spectrum exhibits a peak at 1332 cm^{-1}. And the peaks called *D* band and *G* band are attributed to sp^2-bonded C at 1350cm^{-1} and 1580cm^{-1}. In case of a NCD film, including the peaks of *D* band and *G* band, broad peaks around 1150cm^{-1} and 1475cm^{-1} are exhibited. In figure 1.4.2, the peaks attributed to *D* band and *G* band are presented, but a diamond peak or any peak attributed to NCD is not appeared. Therefore, these films are not considered as diamond films. However, this indicates that absolutely the diamond films are not deposited [37]. In case that the crystallite sizes are too small to be detected, the peak of a diamond could be disappeared. Furthermore, the ratio of the *D* peak to the *G* peak intensity is shown in figure 1.4.4. With increasing the negative bias on the upper metal plate, the ratio of the *D* peak to the *G* peak intensities is increased. This indicates that the bonds of sp^2 domains are broken to be smaller domain sizes.

XRD patterns of the deposited films are shown in figure 1.4.3. The diffraction pattern of the bias voltage of –150V have no definite features both of diamond and graphite. However, with increasing the negative bias voltages on the upper metal plate form –150V to –190V, the reflection peaked at 44.05^o, which is assigned exclusively to the (111) planes of cubic diamond usually observed at 43.9^o, is increased. The reason of the low reflection intensities of diamond (111) plane could be due to small crystal sizes or highly defective structures. Therefore, it is considered that a NCD film with very small grain sizes is synthesized at the substrate temperature of ~430℃ by applying –150V negative DC bias voltage.

A SEM image of NCD film deposited for 21 hours with applying the –190V DC bias voltage is shown in figure 1.4.5. The other deposition conditions were same to the deposition conditions explained in chapter 1.4.1. The growth rate is very slow as 50 nm per one hour.

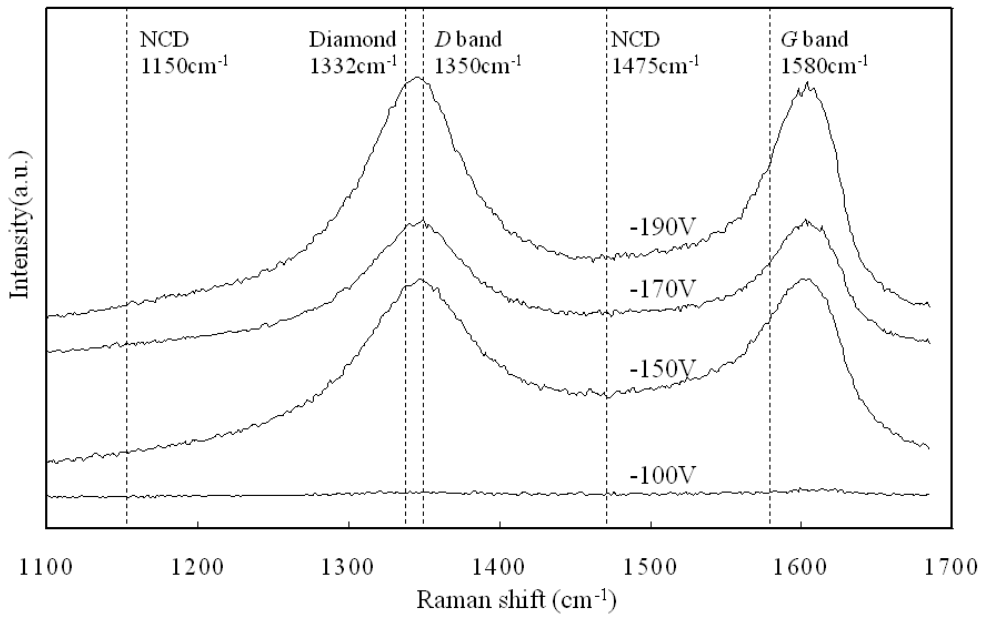

Figure 1.4.2 Raman spectra

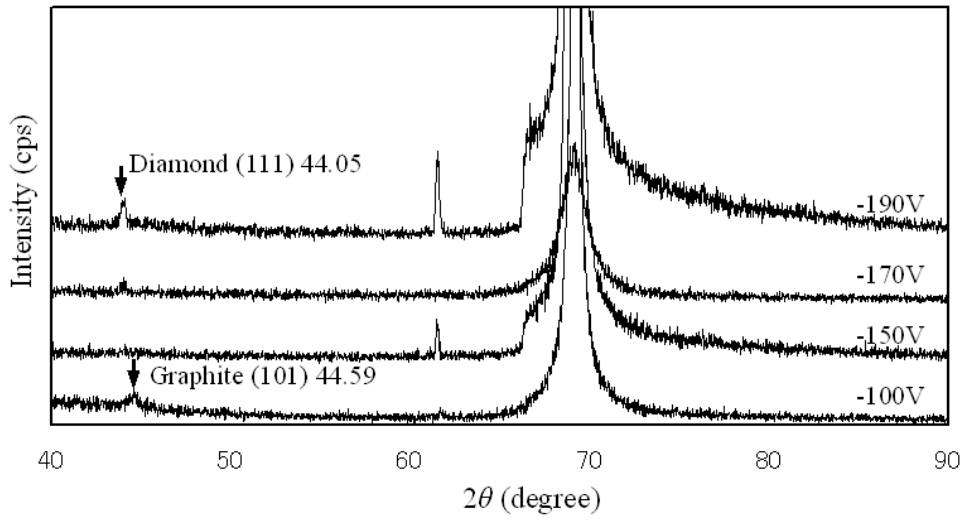

Figure 1.4.3 X –ray diffraction patterns

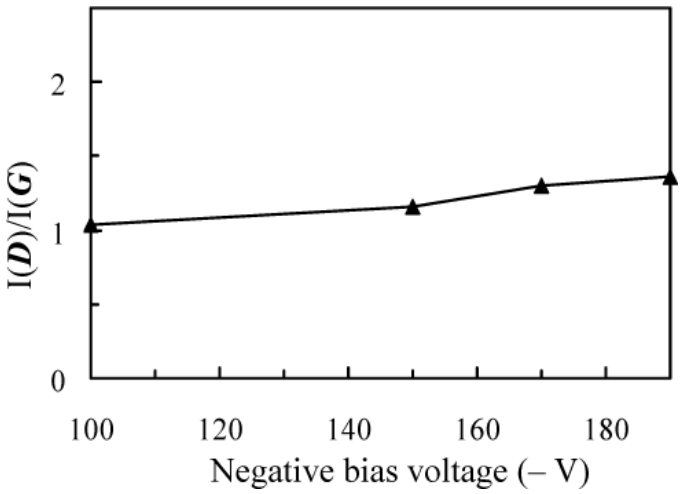

Figure 1.4.4 The ratio of the intensities of *D* peak with respect to the intensities of *G* peak (I(D)/I(G))

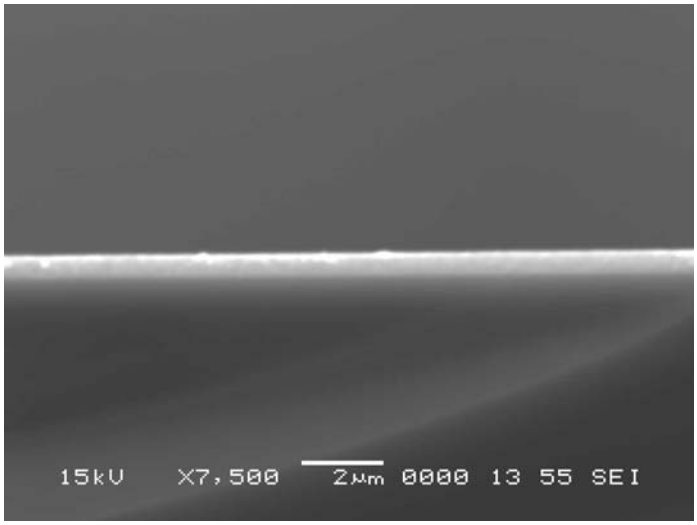

Figure 1.4.5 SEM image of NCD film

1.5. Purpose of this study

A NCD film, which has a high quality of smooth surface (RMS 12.4nm), was synthesized under the conditions of 30mTorr gas pressure, 650℃ substrate temperature, and −70V DC bias voltage in RDL-SWP apparatus with controlling the plasma space potential. And at the previous experiment, a NCD film was achieved at the condition of a low substrate temperature of 430℃, applying the negative bias voltage of –190V to the metal plate inserted under the quartz window (explained in chapter 1.4). From these experimental results, it is considered that there are some relations between the negative DC bias voltages and the substrate temperature on carbon material deposition as shown in figure 1.5.1. Although the plasma potential was saturated at the condition of DC bias voltages under –80V, the characteristics of deposited film was changed at lower DC bias voltages than that. Thus the one more important point is dealing as a function not the plasma potential, but the negative bias voltage.

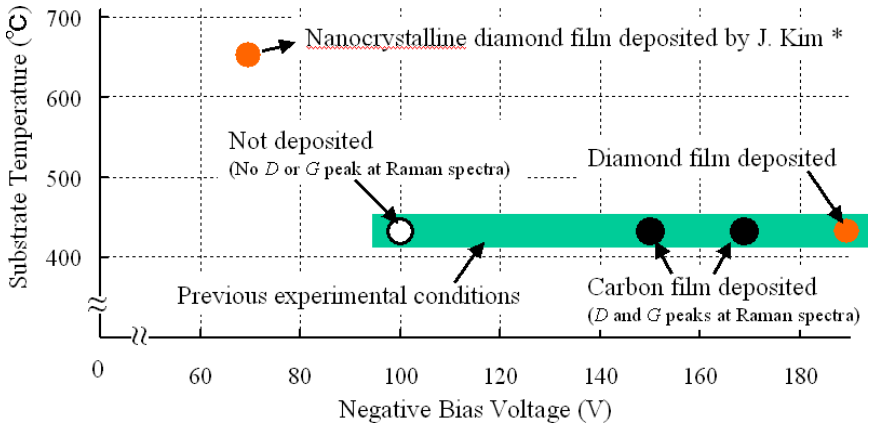

Figure 1.5.1 Summary of previous experiments results

In this study, it is purposed to investigate following three things:

- The relations between DC bias voltages and substrate temperatures on carbon material deposition.
- The dependence of substrate temperature on carbon material deposition
- The dependence of CO gas concentrations on carbon material deposition

To investigate above things, carbon films were synthesized at various conditions as follows:

- DC bias voltages from –80V to –160V at the substrate temperature of 590±5℃ as shown in figure 1.5.2 (A).
- DC bias voltages from –100V to –160V at the substrate temperature of 500±5℃ as shown in figure 1.5.2 (B).
- Substrate temperatures of 645±5℃, 590±5℃, and 500±5℃ at the DC bias voltage of –100V as shown in figure 1.5.2 (C).
- CO gas concentrations of 3%, 4%, and 5% at the substrate temperature of 590±5℃ and the negative bias voltage of –100V

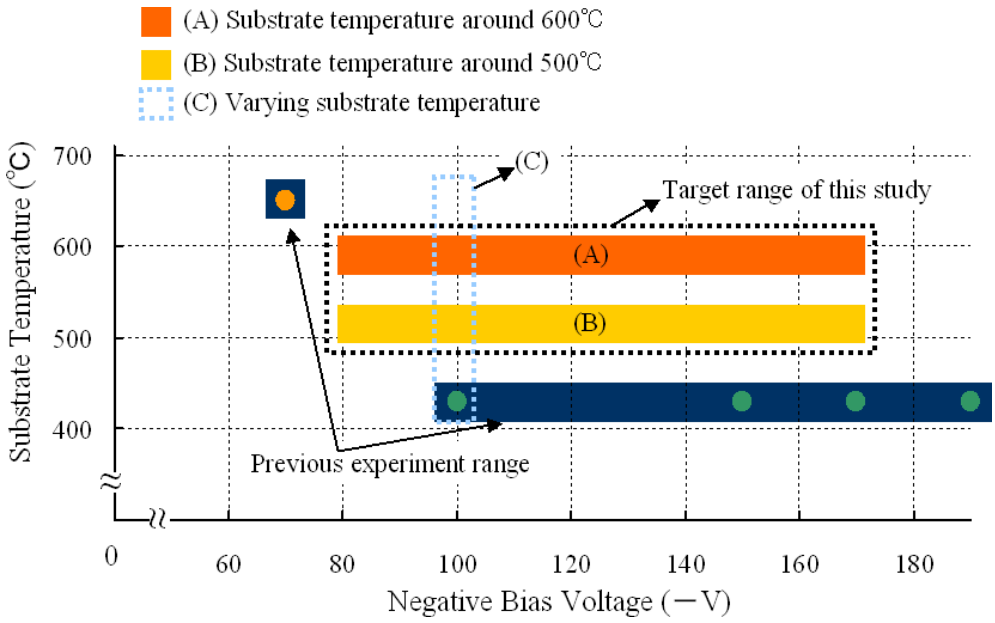

Figure 1.5.2 Experiment conditions for carbon film deposition

2. Negative DC Bias Method

2.1. Introduction

In conventional DC bias method, a positive DC bias voltage is usually applied to the metal substrate holder to reduce the ion bombardment into the substrate. However, this conventional method causes plasma unstableness or arc-like discharges in RDL-SWP apparatus. In this study, a new biasing method developed by J. Kim *et al*. was used [34]. To control the space potential of bulk plasma, a negative bias voltage was applied to the metal plate inserted in the SWP generating region as shown in figure 2.1.1. This new bias method details and formulates theoretically based on the Bohm sheath criterion in the next section

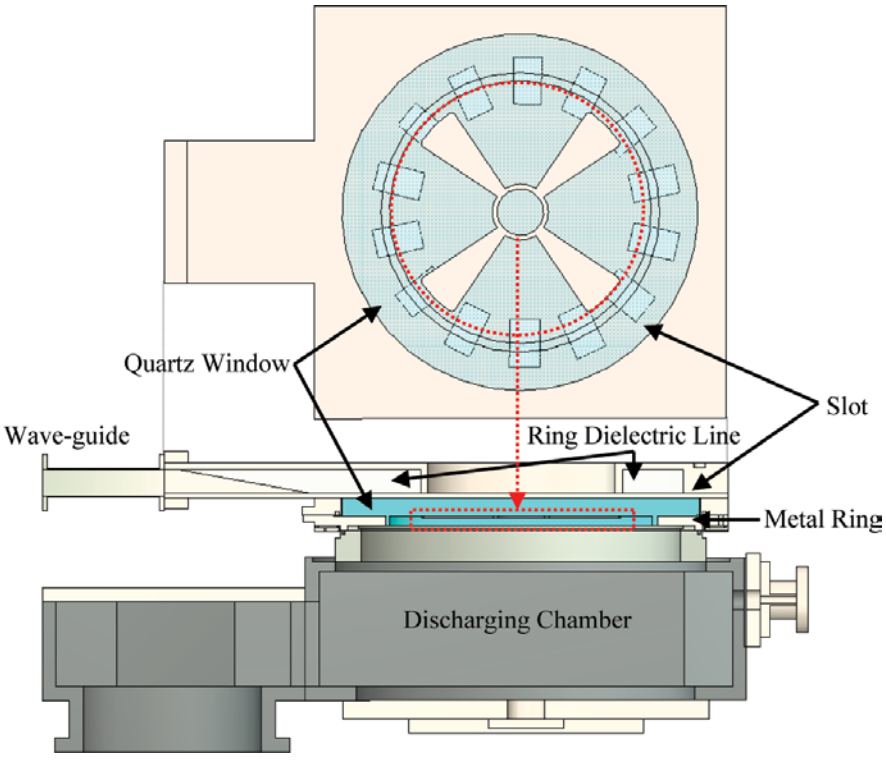

Figure 2.1.1 Schematic illustration of RDL-SWP

2.2. Theoretical analysis of negative DC bias method in RDL-SWP apparatus [1,21]

A simplified theoretical plasma model is considered to describe the mechanism for controlling the space potential of bulk plasma with applying negative bias voltage.

It is assumed that the plasma consists of three separate regions: a thin plasma by surface waves in region A, a bulk plasma in region B, and a transitional plasma between them in region C. And this plasma is connected with lower electrode and upper electrode at the edges of region A and region B. A schematic illustrate is shown in figure 2.2.1.

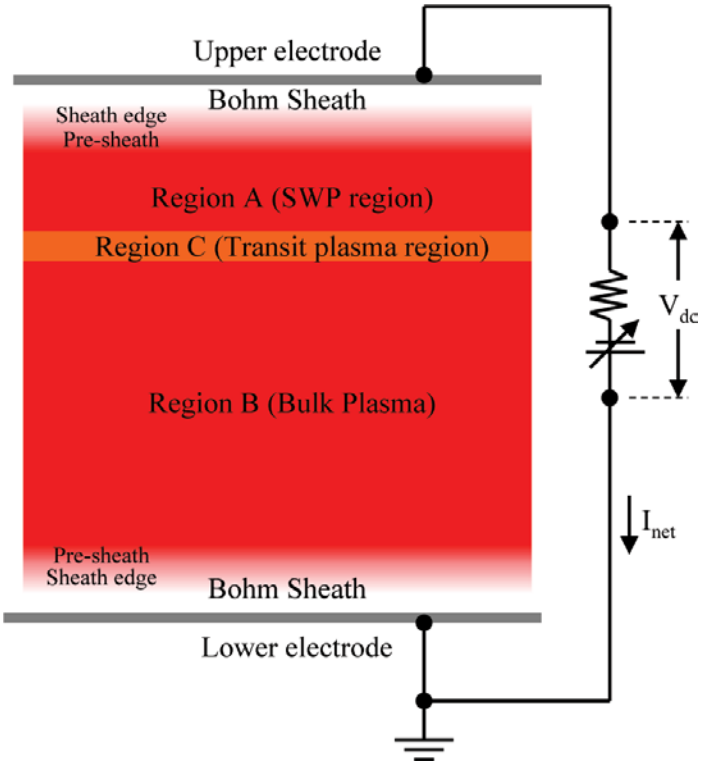

Figure 2.2.1 Schematic illustration of simplified plasma model

2.2.1. The Collisionless Sheath

We use the assumptions as follows;

- Maxwellian electrons at temperature T_e
- Cold ions $T_i = 0$
- $n_e(0) = n_i(0)$ at the plasma-sheath interface at $x = 0$

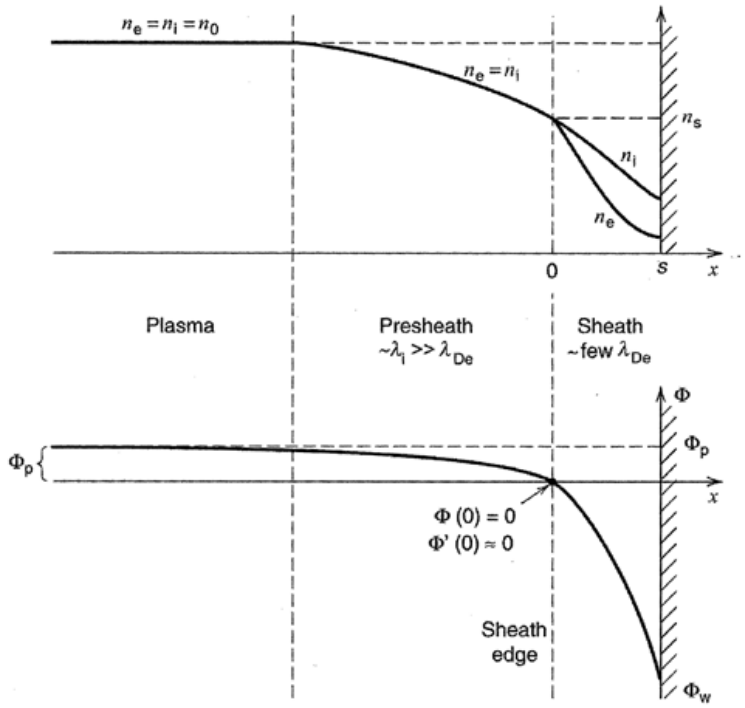

Figure 2.2.2 Qualitative behavior of sheath and presheath in contact with wall [1]

The potential Φ is zero at $x = 0$ and the ions have a velocity u_s there. Then, ion energy conservation gives

$$\frac{1}{2}Mu_s^2 = \frac{1}{2}Mu^2(x) + e\Phi(x). \tag{2.1}$$

The continuity of ion flux (no ionization in the sheath) is

$$n_{is}u_s = n_i(x)u(x), \tag{2.2}$$

where n_{is} is the ion density at the sheath edge.

From (2.2.1) and (2.2.2), we have

$$n_i = n_{is}\left(1 - \frac{2e\Phi}{Mu_s^2}\right)^{-1/2} \tag{2.3}$$

The electron density is given by the Boltzmann relation

$$n_e(x) = n_{es} \exp\left(\frac{\Phi(x)}{\mathrm{T}_e} \right). \tag{2.4}$$

Setting $n_{es} = n_{is} \equiv n_s$ at the sheath edge and substituting n_i and n_e into Poisson's equation, we get

$$\nabla^2 \Phi = -\frac{\rho}{\epsilon_0} \tag{2.5}$$

$$\frac{d^2\Phi}{dx^2} = \frac{e}{\epsilon_0}(n_e - n_i) \tag{2.6}$$

Multiplying by $d\Phi/dx$ and integrating with x and Φ, we obtain

$$\frac{1}{2}\left(\frac{d\Phi}{dx} \right)^2 = \frac{en_s}{\epsilon_0}\left[\mathrm{T_e} \exp\frac{\Phi}{\mathrm{T_e}} - \mathrm{T_e} + 2\mathcal{E}_s\left(1 - \frac{\Phi}{\mathcal{E}_s} \right)^{1/2} - 2\mathcal{E}_s \right] \tag{2.7}$$

The RHS of this equation should be positive for a solution to exist. Thus, we can obtain

$$u_s \geq u_B = \left(\frac{e\mathrm{T_e}}{\mathrm{M}} \right)^{1/2}, \tag{2.8}$$

which is known as the Bohm sheath criterion.

The ions accelerates in a collisionless presheath to the Bohm velocity. Thus the ratio of the density at the sheath edge to that in the plasma is then found the Boltzman relation

$$n_s = n_b \exp\left(-\frac{\Phi_p}{\mathrm{T_e}} \right) \approx 0.61 n_b \tag{2.9}$$

where n_b is the density where the presheath and bulk plasma join.

2.2.2. Current trough the electrode in Region A and Region B

Assuming constant through the sheath, ion flux at the electrode is given by

$$\Gamma_i = n_s u_B . \tag{2.10}$$

And usually electrons are in near-thermal equilibrium at temperature $\mathrm{T_e}$ in discharges, thus the electron flux by considering thermal momentum and Boltzmann's relation is given by

$$\Gamma_e = \frac{1}{4} n_s \bar{v}_e \exp\left(\frac{\Phi_E}{\mathrm{T_e}} \right), \tag{2.11}$$

where

$$\bar{v}_e = \left(\frac{8e\mathrm{T_e}}{\pi m_e} \right)^{1/2}, \tag{2.12}$$

is the mean electron speed and Φ_E is the potential of electrode with respect to the sheath-presheath edge.

Therefore, the ion current I_i and the electron current I_e flowing through the electrode is given by

$$I_i = 0.61 e n_b S_E \left(\frac{e\mathrm{T_e}}{M} \right)^{1/2} \tag{2.13}$$

$$I_e = -\frac{1}{4} e n_b S_E \left(\frac{8e\mathrm{T_e}}{\pi m_e} \right)^{1/2} \exp\left(\frac{\Phi_E}{\mathrm{T_e}} \right) \tag{2.14}$$

where S_E is the area of the electrode surface.

At the electrode, we can obtain the total current through the electrode

$$\begin{aligned} I_E &= I_{iE} + I_{eE} \\ &= 0.61 e n_b S_E \left(\frac{e\mathrm{T_e}}{M} \right)^{1/2} - \frac{1}{4} e n_b S_E \left(\frac{8e\mathrm{T_e}}{\pi m_e} \right)^{1/2} \exp\left(\frac{\Phi_E}{\mathrm{T_e}} \right) \\ &= e n_b S_E \sqrt{e\mathrm{T_e}} \left(0.61 \left(\frac{1}{M} \right)^{1/2} - \frac{1}{4} \left(\frac{8}{\pi m_e} \right)^{1/2} \exp\left(\frac{\Phi_E}{\mathrm{T_e}} \right) \right) \end{aligned} \tag{2.15}$$

At the lower electrode that is grounded electrically, the potential of electrode with respect to the plasma space potential (not sheath-presheath edge) is given by

$$\Phi_{LE} = -\Phi_{pB}, \tag{2.16}$$

where Φ_{pB} is the plasma space potential in region B.

Thus, the total current through the lower electrode is given by

$$I_{LE} = e n_{bB} S_{LE} \sqrt{e\mathrm{T_{e}}_B} \left(0.61 \left(\frac{1}{M} \right)^{1/2} - \frac{1}{4} \left(\frac{8}{\pi m_e} \right)^{1/2} \exp\left(-\frac{\Phi_{pB}}{\mathrm{T_{e}}_B} \right) \right) \tag{2.17}$$

And the potential of electrode with respect to the plasma space potential at the upper electrode is given by

$$\Phi_{UE} = \Phi_b - \Phi_{pA} \tag{2.18}$$

where Φ_b is the bias voltage applied to the upper electrode and Φ_{pA} is the plasma space potential in region A.

The total current through the upper electrode is obtained as

$$I_{UE} = en_{bA}S_{UE}\sqrt{e\mathrm{T}_{\mathrm{e}A}}\left(0.61\left(\frac{1}{M}\right)^{1/2} - \frac{1}{4}\left(\frac{8}{\pi m_e}\right)^{1/2}\exp\left(\frac{\Phi_b - \Phi_{pA}}{\mathrm{T}_{\mathrm{e}A}}\right)\right) \tag{2.19}$$

Since $I_{UE} + I_{LE} = 0$, we obtain

$$\begin{aligned} I_{LE} + I_{UE} &= en_{bB}S_{LE}\sqrt{e\mathrm{T}_{\mathrm{e}B}}\left(0.61\left(\frac{1}{M}\right)^{1/2} - \frac{1}{4}\left(\frac{8}{\pi m_e}\right)^{1/2}\exp\left(-\frac{\Phi_{pB}}{\mathrm{T}_{\mathrm{e}B}}\right)\right) \\ &\quad + en_{bA}S_{UE}\sqrt{e\mathrm{T}_{\mathrm{e}A}}\left(0.61\left(\frac{1}{M}\right)^{1/2} - \frac{1}{4}\left(\frac{8}{\pi m_e}\right)^{1/2}\exp\left(\frac{\Phi_b - \Phi_{pA}}{\mathrm{T}_{\mathrm{e}A}}\right)\right) \\ &= 0 \end{aligned} \tag{2.20}$$

3. Experimental setup

3.1. Surface wave plasma apparatus

In this study, Ring Dielectric Line (RDL) typed SWP apparatus (shown in figure 3.1.1), which had been developed by Sumitomo Metal Co. in Japan, was employed as a Plasma CVD apparatus for carbon film depositions. The cross sectional schematic illustration of RDL-SWP apparatus is shown in figure 3.1.2.

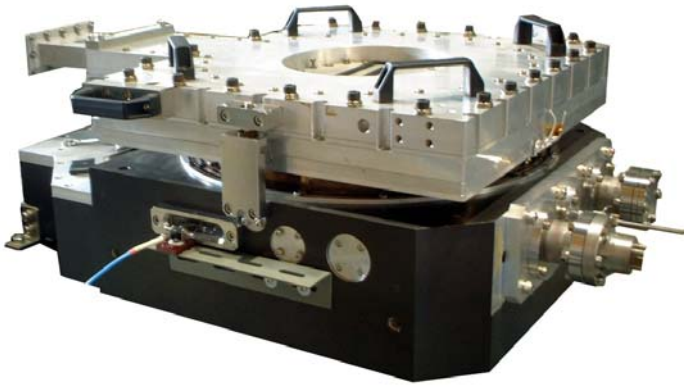

Figure 3.1.1 Picture of RDL-SWP

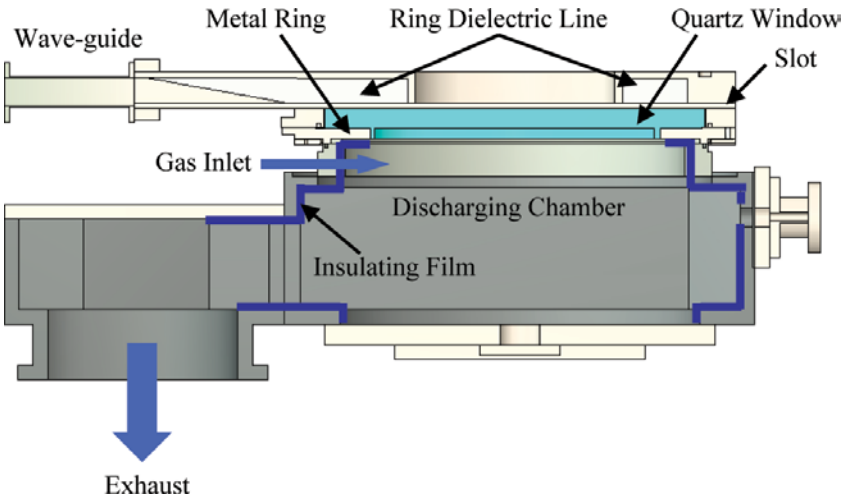

Figure 3.1.2 Cross sectional schematic illustration of RDL-SWP

3.1.1. Discharging mechanism

The incident microwave traveled along waveguides with the frequency of 2.45 GHz propagates through the ring dielectric line, and produces a standing wave in the ring dielectric line. And then, the power introduced by electromagnetic waves is transmitted to the discharging chamber through the metal slots and the quartz disk window under the ring dielectric line. At first, discharges exited under the metal slots and expanded to the center of the discharging chamber due to the influence of the metal ring. And the plasma sustained by surface waves, which propagate along the interface between plasma and quartz disk window, is generated (Shown in figure 3.1.3).

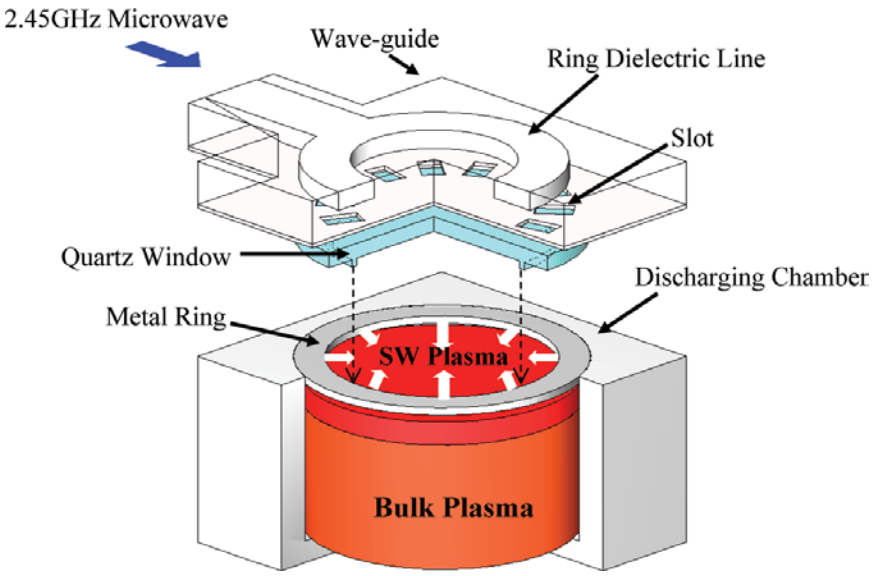

Figure 3.1.3 Discharging mechanism in RDL-SWP apparatus

3.1.2. Modification for applying DC bias voltage

Figure 3.1.4 shows a cross sectional schematic illustration of the modified RDL-SWP apparatus. To control the space potentials in the bulk plasma region, a metal plate inserted under quartz disk window. This metal plate deigned for promoting the propagation of SW into the center of the discharging chamber and providing high electron densities in the CVD region. The sidewall of the discharging chamber was coated with insulation films. And a metal vessel was inserted and electrically floated from the sidewall and bottom plate of the discharging chamber. A heater which has a heating ability to ~700℃ was inserted as a substrate holder to control the substrate temperature, and it was grounded electrically.

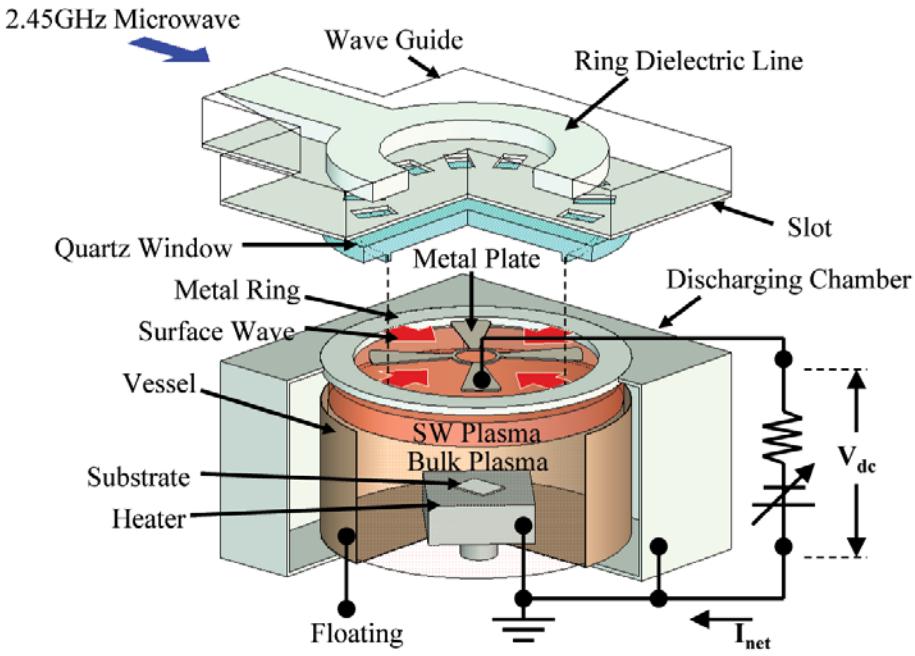

Figure 3.1.4 Schematic illustration of modified RDL-SWP

3.2. Plasma parameters measurement

3.2.1. Single probe measurement

Plasma parameters such as electron densities, electron temperatures and space potentials were measured by single probe method that is well known as Langmuir probe method. . The tip of probe was made of a cylindrical tungsten wire dimensioned by diameter of 1.25 mm and length of 1.5 mm, and electrically isolated from the outer stainless-steel pipe by another alumina pipe. The experimental setup for measuring with single probe method is shown in figure 3.2.1.

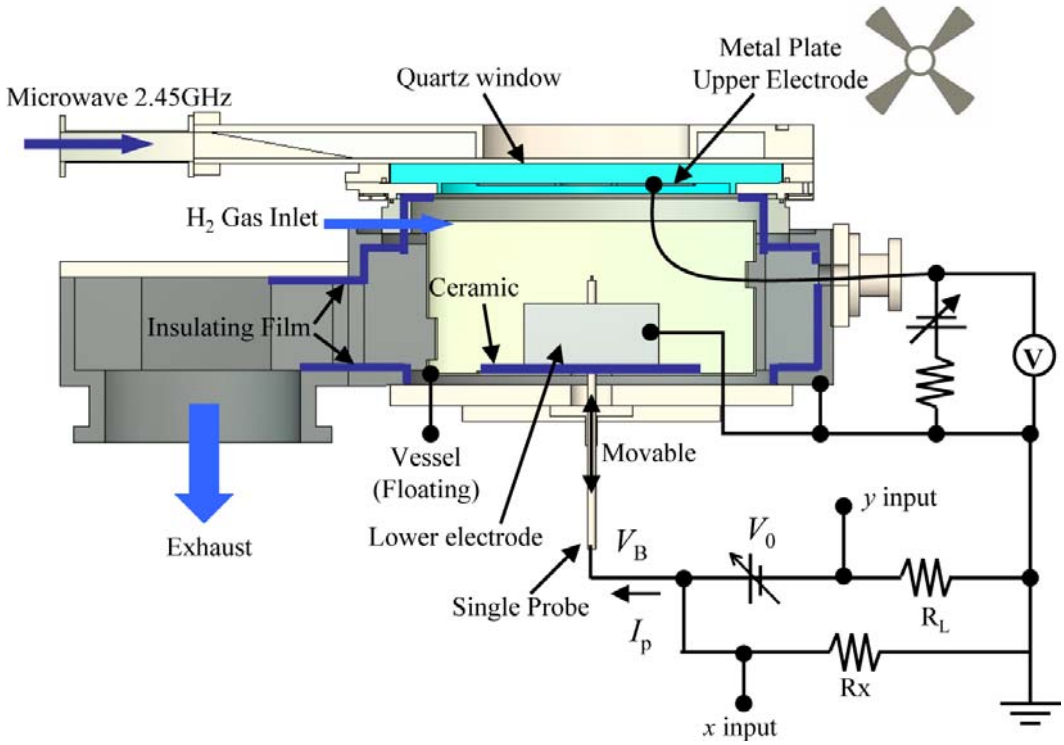

Figure 3.2.1 Schematic illustration of experimental setup

Applying varying voltages to the single probe with respect to the grounded discharging chamber, the change in currents with voltage was measured. This gives a typical probe voltage-current characteristic curve. Taking the logarithm of current, a curve of the logarithmic current vs. voltage can be redrawn. The electron temperature is obtained directly from the inverse slope of that curve as shown in figure 3.2.2. And the plasma potential and the electron saturation current can be also obtained from the point of maximum first derivate of that curve.

Then the electron density can be calculated by given equation of

$$n_e = \frac{4}{e}\frac{I_{es}}{S_p}\sqrt{\frac{\pi m_e}{8kT_e}}, \tag{2.1}$$

where e is the elementary charge, I_{es} is the electron saturation current, S_p is the probe surface area, m_e is the electron mass, k is the Bolzmann constant, and T_e is the electron temperature.

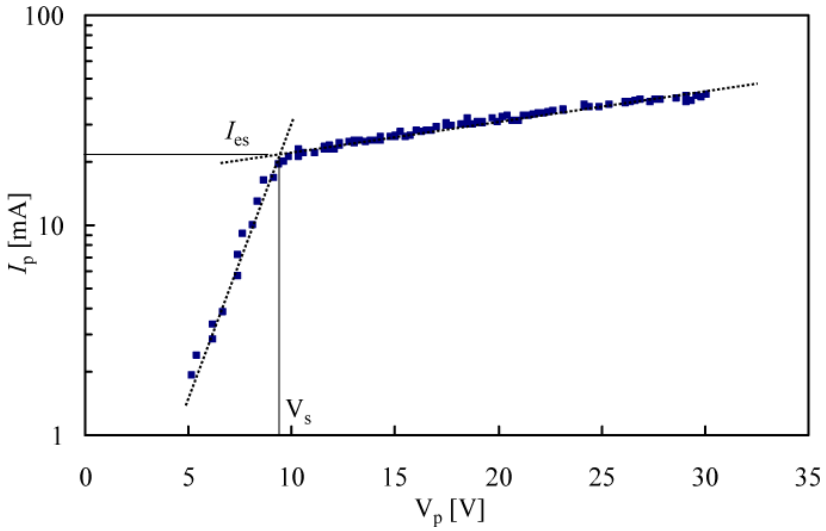

Figure 3.2.2 Probe voltage vs. logarithmic current characteristic curve

3.3. Synthesis of carbon films

3.3.1. Carbon film depositions

The modified RDL-SWP apparatus explained in chapter 3.1.2 was used to synthesize carbon films as plasma CVD apparatus. Basically, the structure of RDL-SWP apparatus was same to the one of the previous experiments explained in chapter 1.4.

As shown in figure 3.3.1, a thermocouple was attached to measure the substrate temperature on the surface of the heater. And using a temperature controller, the substrate temperature was controlled at any inserted value ±5℃.

Likewise, n-type mirror polished silicon (100) was used as a substrate. And any pre-treatment for nucleation of diamond was not performed. Using MFC system, the gas mixture of 95%H2-5%CO was injected as source gas except the experiments for investigating the dependence of CO gas concentration. The optical emission intensity of radicals was checked for every experiment to keep the initial experimental condition from the effects of contaminated discharging chamber wall.

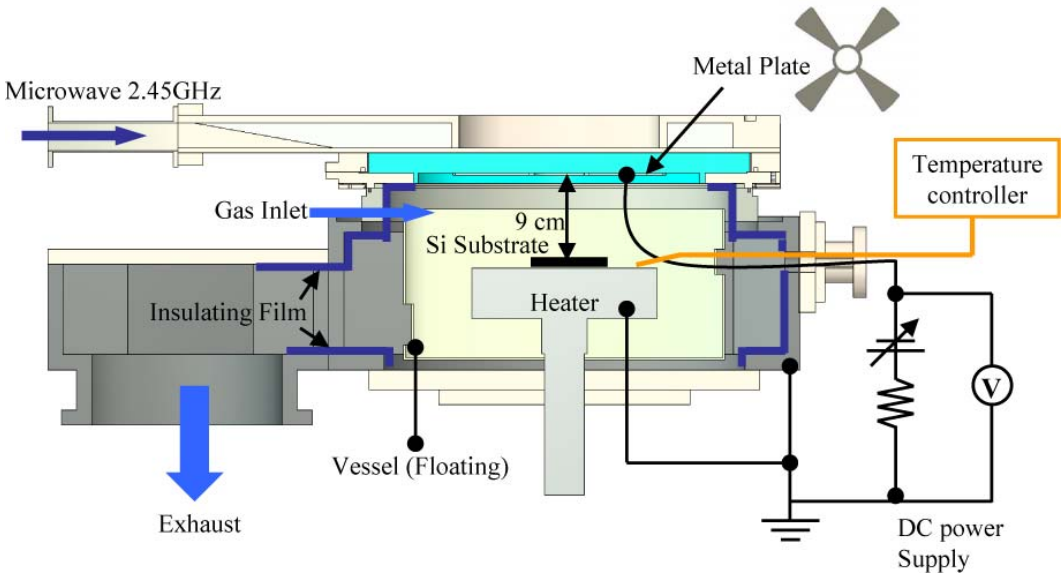

Figure 3.3.1 Schematic illustration of experimental setup

4. Plasma Parameters in RDL-SWP Apparatus

4.1. Plasma parameters in H2 gas with applying negative DC bias voltages

Plasma parameters such as electron densities, electron temperatures and space potentials were measured with applying negative DC bias voltages to the inserted metal plate by single probe method explained in chapter 3.2.

The schematic illustration of experimental setup is shown in Fig. 4.1.1. An electrode that has a same surface area with the heater used as substrate holder was inserted. And it was placed on ceramic plate to isolate electrically from the bottom of the RDL-SWP apparatus. The probe was inserted from the bottom of apparatus and the tip of probe was placed in CVD region where is 9 cm off from the quartz window. 100%H_2 gas was injected and the gas pressure was preserved as 30 mTorr in discharging chamber. Negative DC bias voltages were applied to the metal plate (upper electrode) from 0V to –180V.

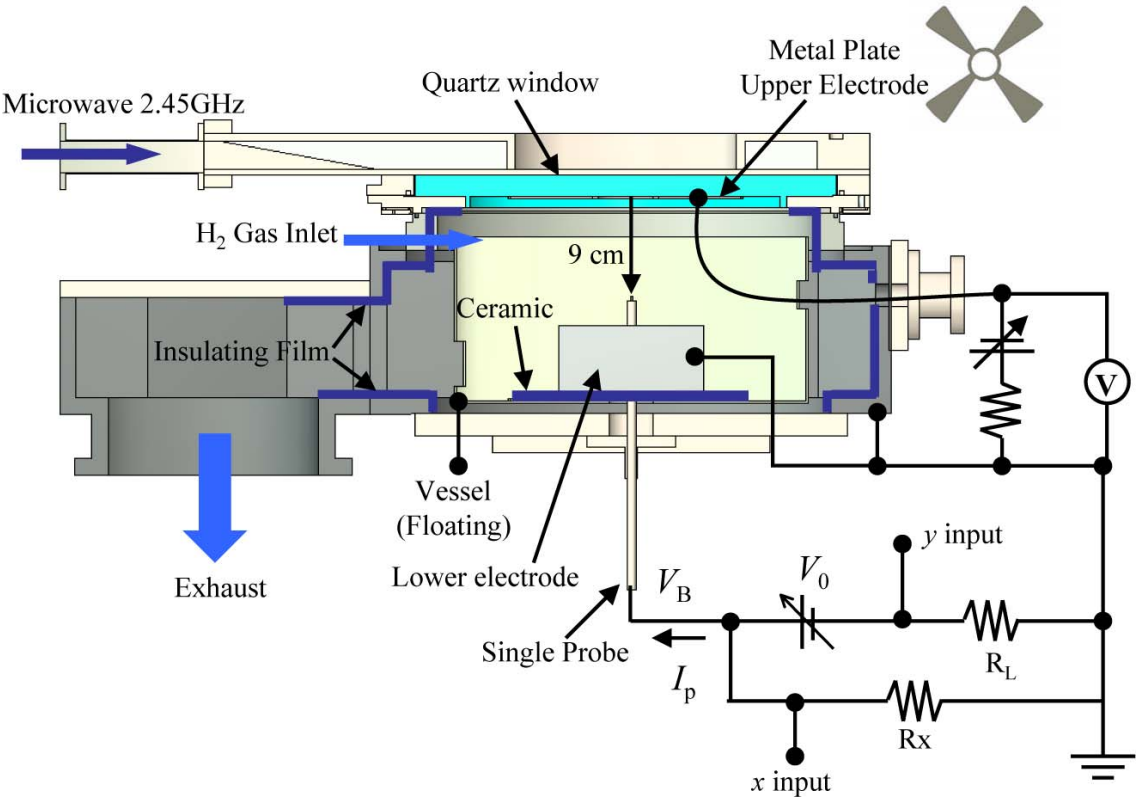

Figure 4.1.1 Schematic illustration of experimental setup

The measurement results are shown in figure 4.1.2. The variation of electron densities with respect to the negative bias voltage applied to the upper metal plate is shown in figure 4.1.2. (a). As the result, the electron temperature was decreased from 3.03eV to1.92eV with increasing the negative DC bias voltage. On the other hand, according to figure 4.1.2. (b), the electron density was increased from $2.3\times10^{10}cm^{-3}$ to $3.0\times10^{10}cm^{-3}$ with increasing the negative DC bias voltage. The space potential of bulk plasma was 16.3V at the negative DC bias voltage of 0V (both electrodes was linked electrically). With increasing the negative bias voltage, the space potential was decreased to ~11V. However, as the net current flowing through the electrodes was saturated at the negative bias voltage of ~80V, the space potential in bulk plasma was also saturated at ~11V.

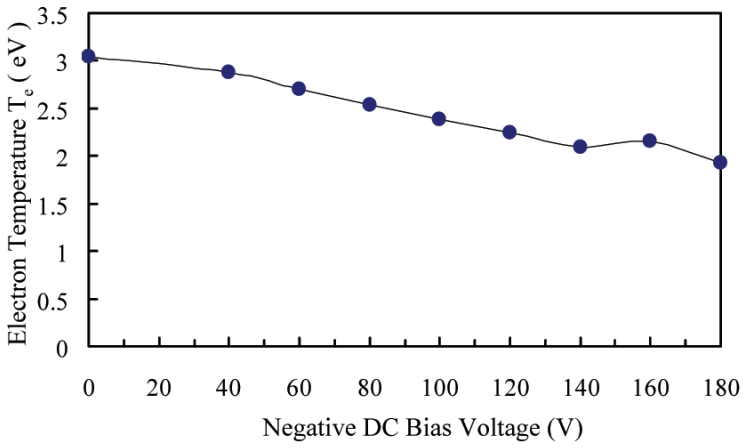

(a) Electron temperatures

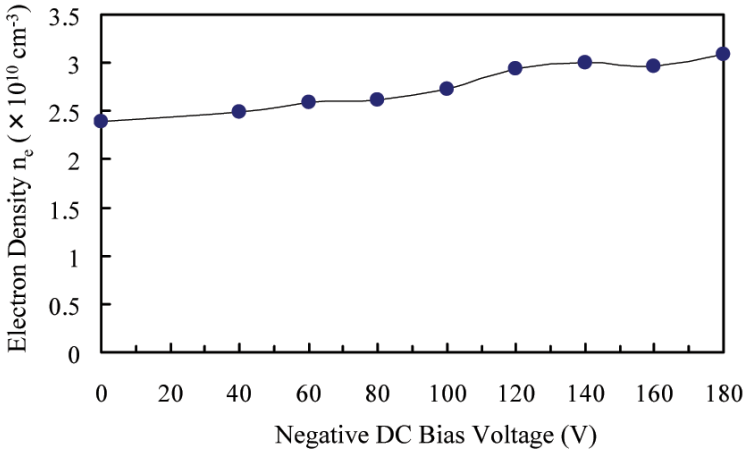

(b) Electron densities

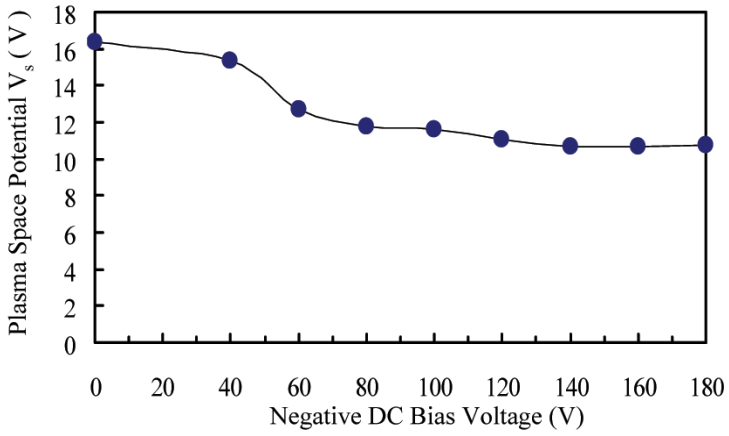

(c) Plasma space potentials

Figure 4.1.2 Plasma parameters in bulk plasma

5. Carbon Film Deposition

5.1. Introduction

To investigate the influences of negative bias voltage and substrate temperature on carbon film deposition, carbon films were synthesized under the condition of different bias voltages and different substrate temperatures as shown in figure 5.1.1. And the deposited films were analyzed by Ar+ laser Raman spectroscopy, ultra violet Raman spectroscopy, field emission scanned electron microscopy, and X-ray diffraction. In chapter 5.2, the measurement results of the films, which were deposited at the substrate temperature of 590±5℃ and 500±5℃ with applying the DC bias voltages from –80V to –170V, are presented. From these results, the relations between negative bias voltages and substrate temperatures on carbon film deposition are discussed. In chapter 5.3, with the measurement results of films deposited under the condition of –100V DC bias voltage and the substrate temperature of 645±5℃, 590±5℃, and 500±5℃. And the dependences of substrate temperatures on carbon film deposition are discussed. In chapter 5.4, the measurement results of the films deposited at the condition of different CO concentrates in source gas are presented. And the dependences of CO gas concentrations on carbon films deposition are discussed.

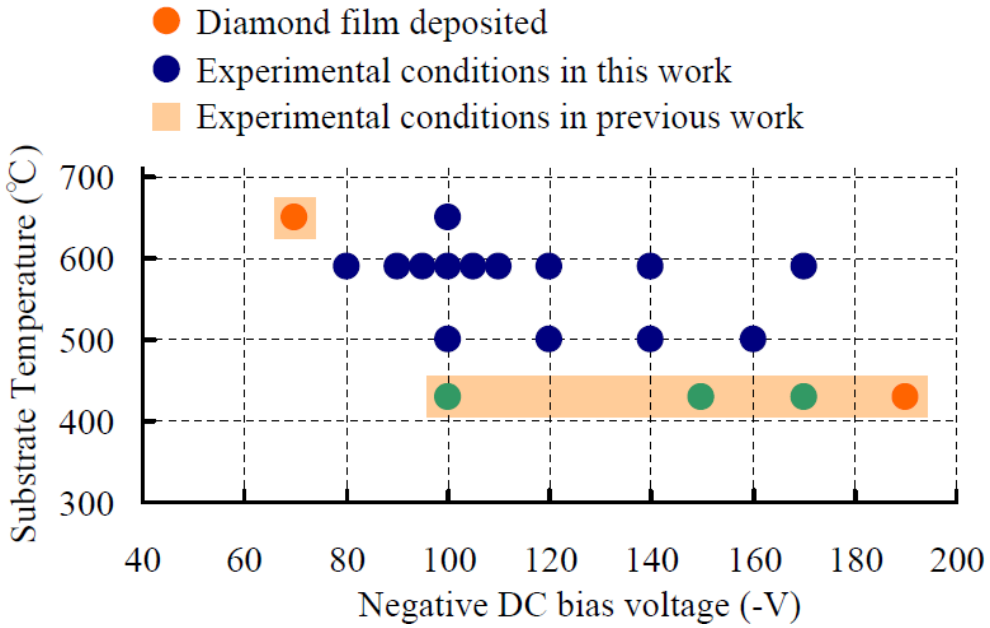

Figure 5.1.1 Experimental condition

5.2. Characteristics of carbon films deposited at different DC bias voltages

Using RDL-SWP apparatus with applying negative DC bias voltages to the upper metal plate, synthesis of carbon films were carried out under the condition of different bias voltages from –80V to –160V. As the substrate for deposition, n-type mirror-polished silicon (100) was used. The substrates were just cleaned in methanol vessel without any pre-treatment for the nucleation of diamond, and placed on the substrate holder (heater) grounded electrically. And as source gas, a gas mixture of 95%H_2–5%CO was injected to the discharging chamber and the gas pressure was preserved as 30±2 mTorr. The incident microwave power was preserved at 1.49±0.01kW and the substrate temperatures were controlled as 590±5℃ and 500±5℃. The characteristics of these synthesized films were analyzed by Ar+ laser Raman spectroscopy, UV Raman spectroscopy, X-ray diffraction, and field emission scanning electron microscope (FE-SEM).

5.2.1. substrate temperature around 590℃

The experimental details performed at the substrate temperature of 590±5℃ are shown in table 5.2.1

Table 5.2.1 Experimental conditions

NO.	DC Bias voltage (V)	Source gas (%) H2	CO	Duration (hour)
1	– 80	95	5	7.2
2	– 100	95	5	7
3	– 120	95	5	7.2
4	– 140	95	5	7
5	– 170	95	5	7

The Ar+ laser Raman spectra of the deposited films is shown in figure 5.2.1. Usually, Raman spectrum exhibits a sharp peak at 1332 cm^{-1} in case of natural diamond, but in the figure of 5.2.1, no diamond peak is presented. However, the peaks called *D* peak and *G* peak attributed to sp^2-bonded C, are presented at 1350cm^{-1} and 1580cm^{-1} respectively. And these *D* and *G* peaks were intensified with increasing the negative bias voltages.

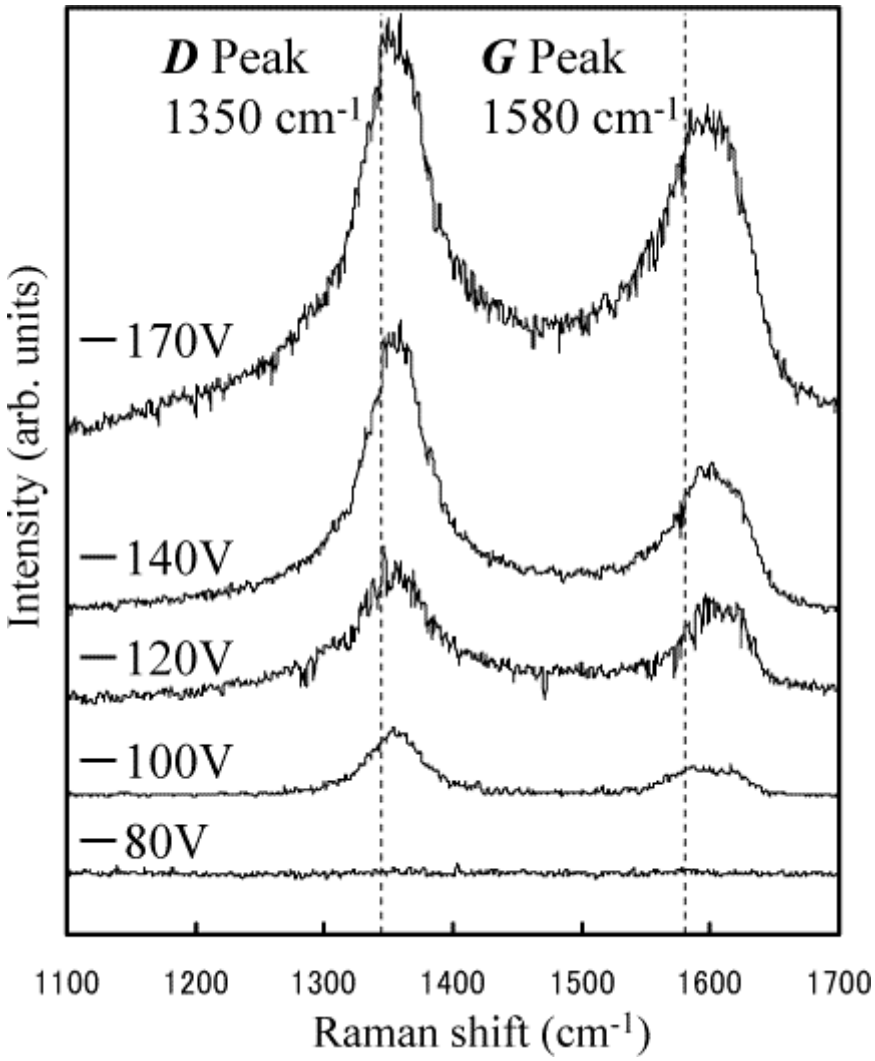

Figure 5.2.1 Ar+ laser Raman Spectra

The *G* mode is actually stretching vibration mode of any pair of sp^2 sites, whether in C=C chain or in aromatic rings. However, the *D* mode is the breathing mode of sp^2 sites only in rings, not chain. Thus, the intensity ratio of *D* and *G* peak is proportional to the number of rings at the edge of the grain. And in figure 5.2.2, the intensity of *D* peak against the intensity of *G* peak was calculated and was plotted as a function of DC bias voltage [27].

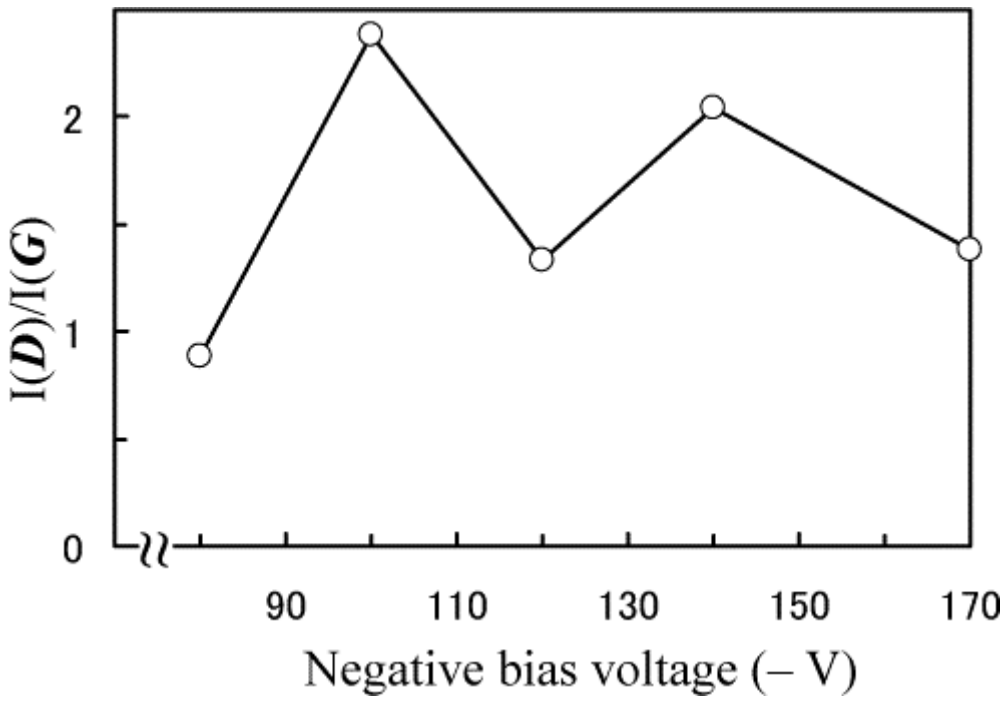

Figure 5.2.2 Ratio of *D* peak against *G* peak (I(D)/I(G))

In figure 5.2.2, increasing the bias voltages, *D* peak is bigger than *G* peak at all bias voltages and the ratio of *D* and *G* peaks tends downwards. These indicate that the sp^2 domains are discretized to small domains and the grain sizes are decreased. The amorphisation is also promoted simultaneously.

These facts can be confirmed by the results of UV Raman spectra in figure 5.2.3. At the bias condition of over –120V, the *G* peak is changed a broad peak. This means the grain sizes were decreased.

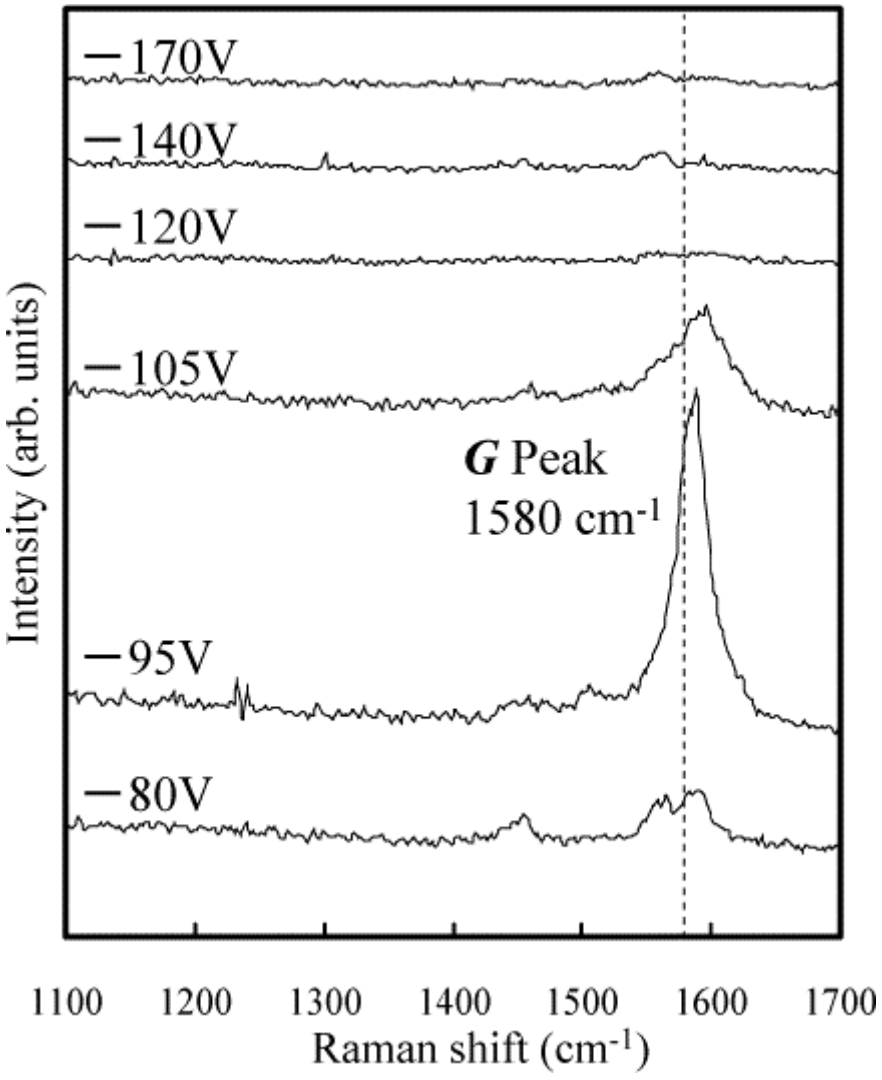

Figure 5.2.3 UV Raman spectra

In previous experiment explained in chapter 1.4, we could achieve a diamond peak in XRD patterns, although there is no diamond peak in Raman spectra. Thus, the XRD measurement was carried out and shown in figure 5.2.4. However, no diamond peak was exhibited at whole deposition conditions. This indicates that the deposited films are not to be crystallized.

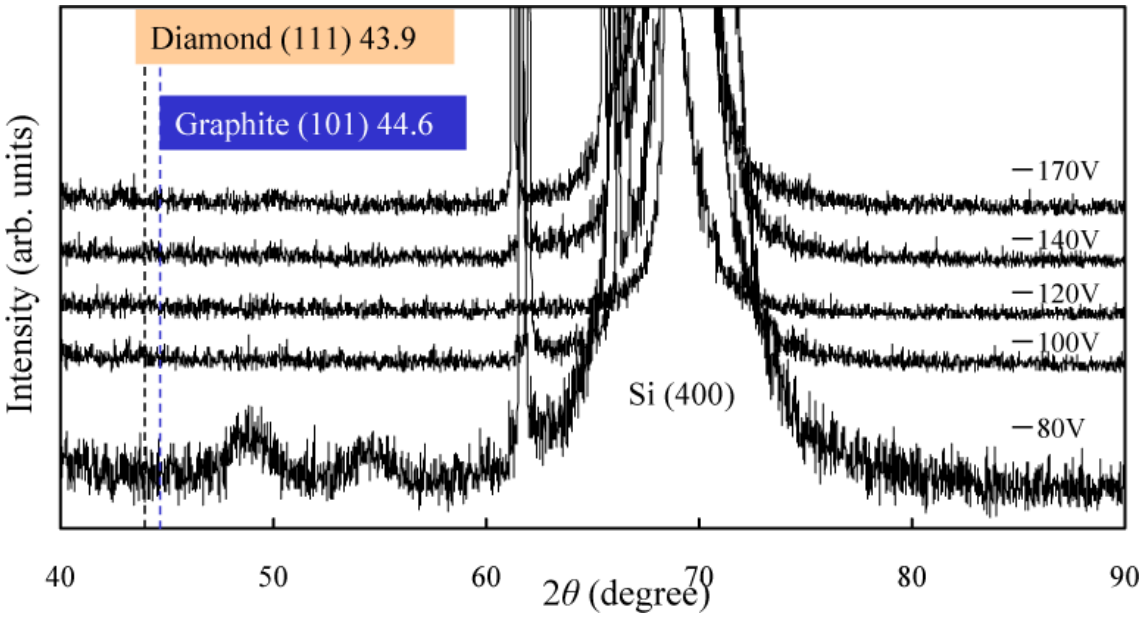

Figure 5.2.4 XRD patterns

With the result of FE-SEM measurement, interesting film morphology was founded. The deposited films were very flat and continuous morphology with grains sized 20nm approximately. And at some region where has damages on substrate, grains looks like diamond were founded as shown in figure 5.2.5. Maybe the diamond peak achieved in UV Raman spectra is due to measuring this region.

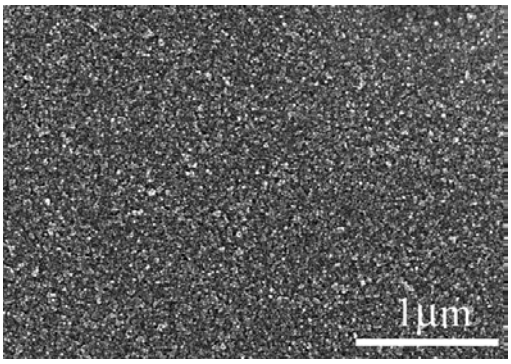

(a) –100V bias voltages

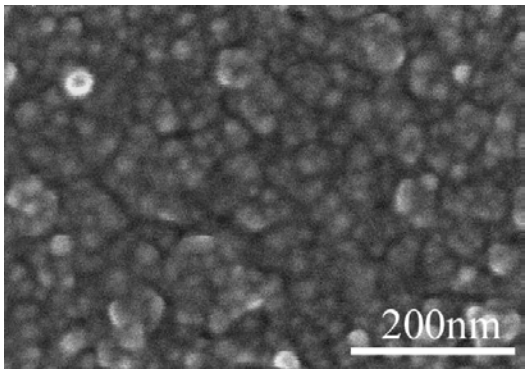

(b) –100V bias voltages

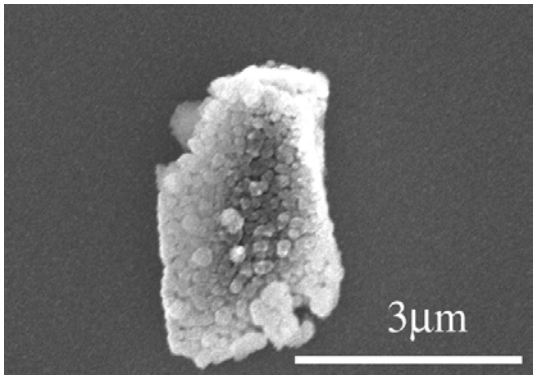

(c) –100V bias voltages

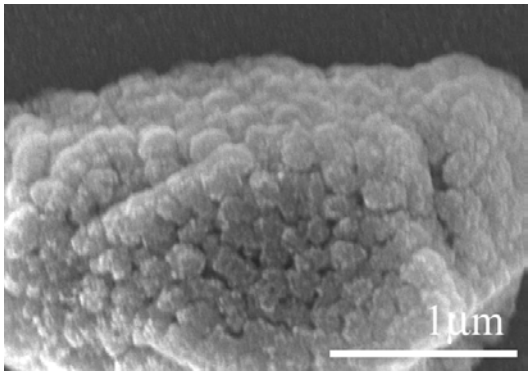

(d) –100V bias voltages

Figure 5.2.5 FE-SEM Images

5.2.2. substrate temperature around 500℃

And the carbon film deposition experiments were carried out at the lower substrate temperature. The experimental details performed at the substrate temperature of 500±5℃ are shown in table 5.2.2

Table 5.2.2 Experimental conditions

NO.	DC Bias voltage (V)	Source gas (%) H2	CO	Duration (hour)
1	– 100	95	5	7.3
2	– 120	95	5	8
3	– 140	95	5	7.6
4	– 160	95	5	7.6

The Ar+ laser Raman spectra of the deposited films is shown in figure 5.2.6. As same to previous results, no diamond peak is presented. The peaks of *D* peak and *G* peak are presented at 1350cm^{-1} and 1580cm^{-1} respectively. These *D* and *G* peaks were intensified with increasing the negative bias voltages.

And in figure 5.2.7, the ratio of *D* peak with respect to the intensity of *G* peak was calculated and plotted as a function of DC bias voltage.

The intensities of *D* peaks are stronger than the intensities of *G* peaks at these deposition conditions as shown in figure 5.2.7. This indicates that the sp^2 domains are discretized to small domain and the grain sizes are very small. And as shown in figure 5.2.8, this change of deposited film morphology is very similar to the one of substrate temperature 590±5℃, but appeared at lower DC bias voltages than that.

These facts are also confirmed by the result of UV Raman spectra in figure 5.2.8. At the bias condition of over –140V, the *G* peaks is changed a broad peak.

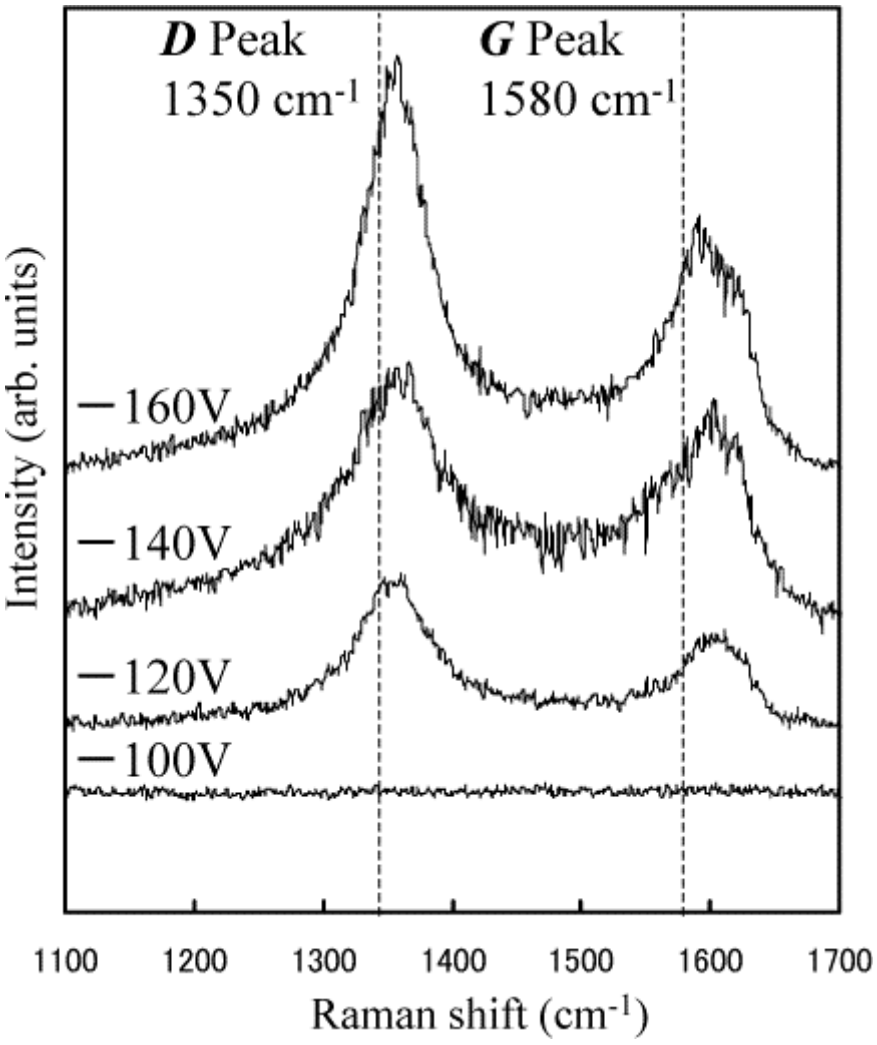

Figure 5.2.6 Ar+ laser Raman spectra

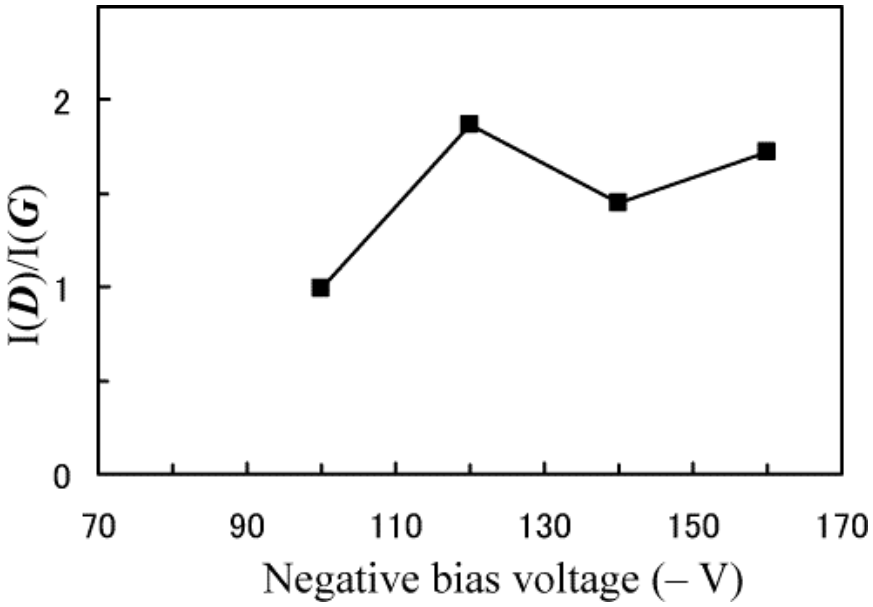

Figure 5.2.7 Ratio of D peak against G peak (I(D)/I(G))

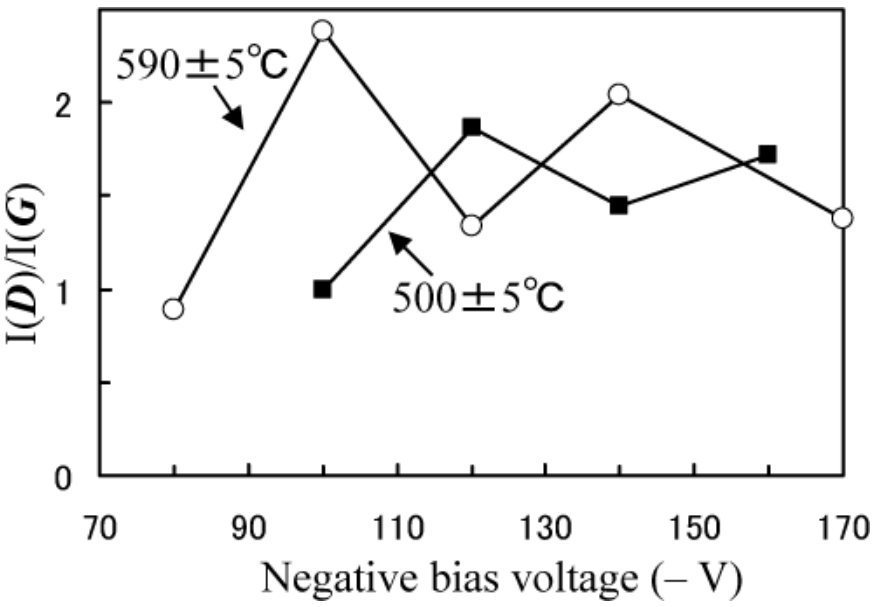

Figure 5.2.8 Ratio of *D* peak against *G* peak (I(D)/I(G))

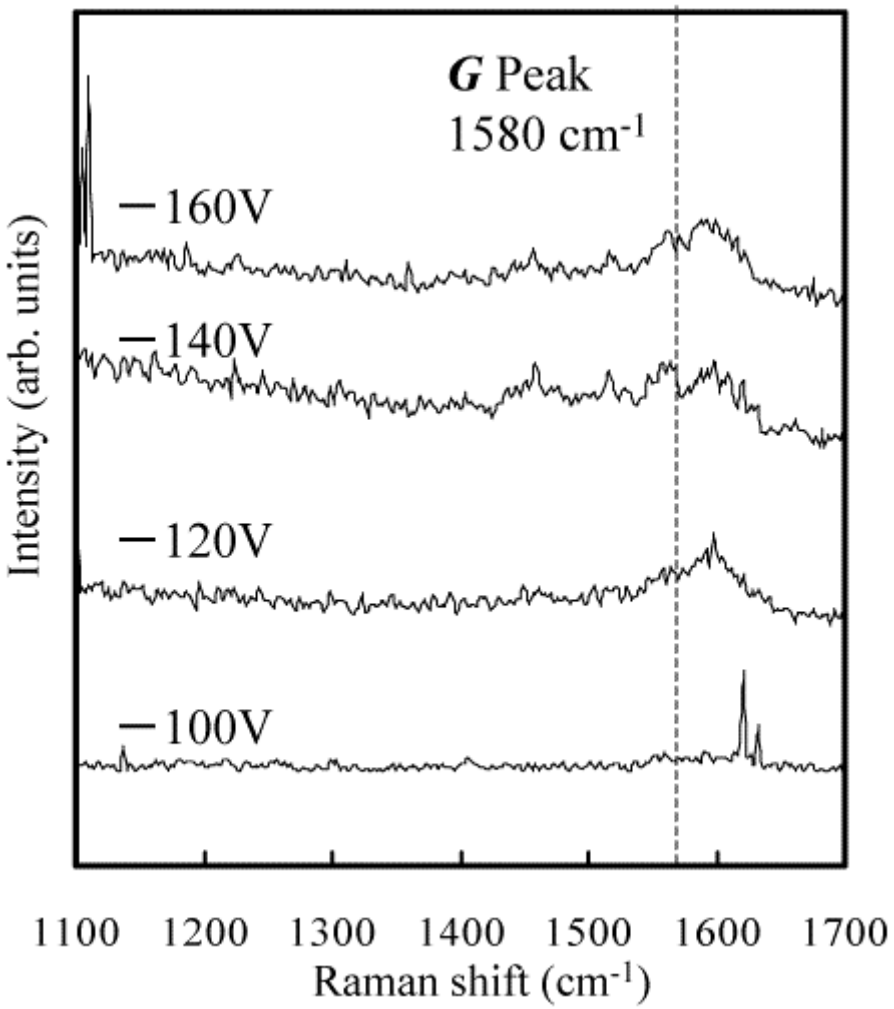

Figure 5.2.9 UV Raman spectra

As same the films deposited at substrate temperature 590±5℃, no diamond peak is exhibited in figure 5.2.10. This indicates that the deposited films are not to be crystallized.

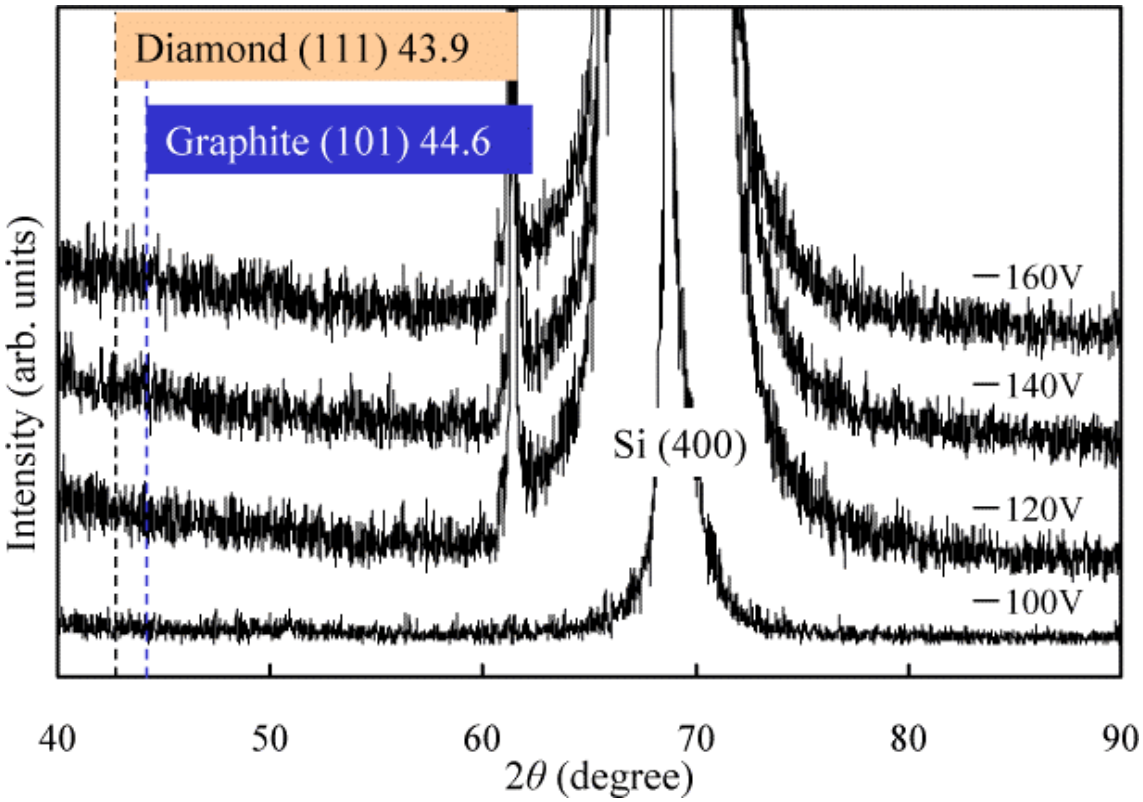

Figure 5.2.10 XRD patterns

5.3. Characteristics of carbon films deposited at different substrate temperature

Synthesis of carbon films were carried out under the conditions of different substrate temperatures of 650±5℃, 590±5℃, and 500±5℃ with applying DC bias voltage of –100V to the upper metal plate in RDL-SWP apparatus.

As a substrate, evenly n-type mirror-polished silicon (100) was used. The substrates were just cleaned in methanol without any pre-treatment for the nucleation of diamond, and placed on the substrate holder (heater) grounded electrically. And a gas mixture of 95%H2–5%CO was injected to the discharging chamber and the gas pressure was preserved as 30±2 mTorr. The deposited films were analyzed by Ar+ laser Raman spectroscopy and FE-SEM.

The experimental conditions are shown in table 5.3.1

Table 5.3.1 Experimental conditions

NO.	Substrate Temperature (℃)	Source gas (%)		Duration (hour)
		H2	CO	
1	650±5℃	95	5	7
2	590±5℃0	95	5	7.5
3	500±5℃	95	5	7.3

The Ar+ laser Raman spectra of the deposited films is shown in figure 5.3.1. The *D* peaks and *G* peaks are presented at 1350cm^{-1} and 1580cm^{-1}, respectively. These *D* and *G* peaks were intensified with increasing the substrate temperature from 500±5℃ to 590±5℃. But intensities of the *D* peak and *G* peak were inversed at the substrate temperature of 650±5℃.

The ratio of the intensity of *D* peak against the intensity of *G* peak was calculated and plotted as a function of DC bias voltage in figure 5.3.2.

Because the carbon film deposited has very weak intensities of *G* and *D* peak, the ratio of I(D)/I(G) is approximately 1 at the substrate temperature of 500±5℃. It looks like the ratio of I(D)/I(G) is increased with increasing the substrate temperature from 500±5℃ to at 650±5℃. However, this does not result from small grain size or increasing of sp^2 domain. And the ratio of I(D)/I(G) is decreased significantly at substrate temperature of 650±5℃. According to FE-SEM images in figure 5.3.3, the intensity of *G* peak was increased due to the wall-like graphite structure.

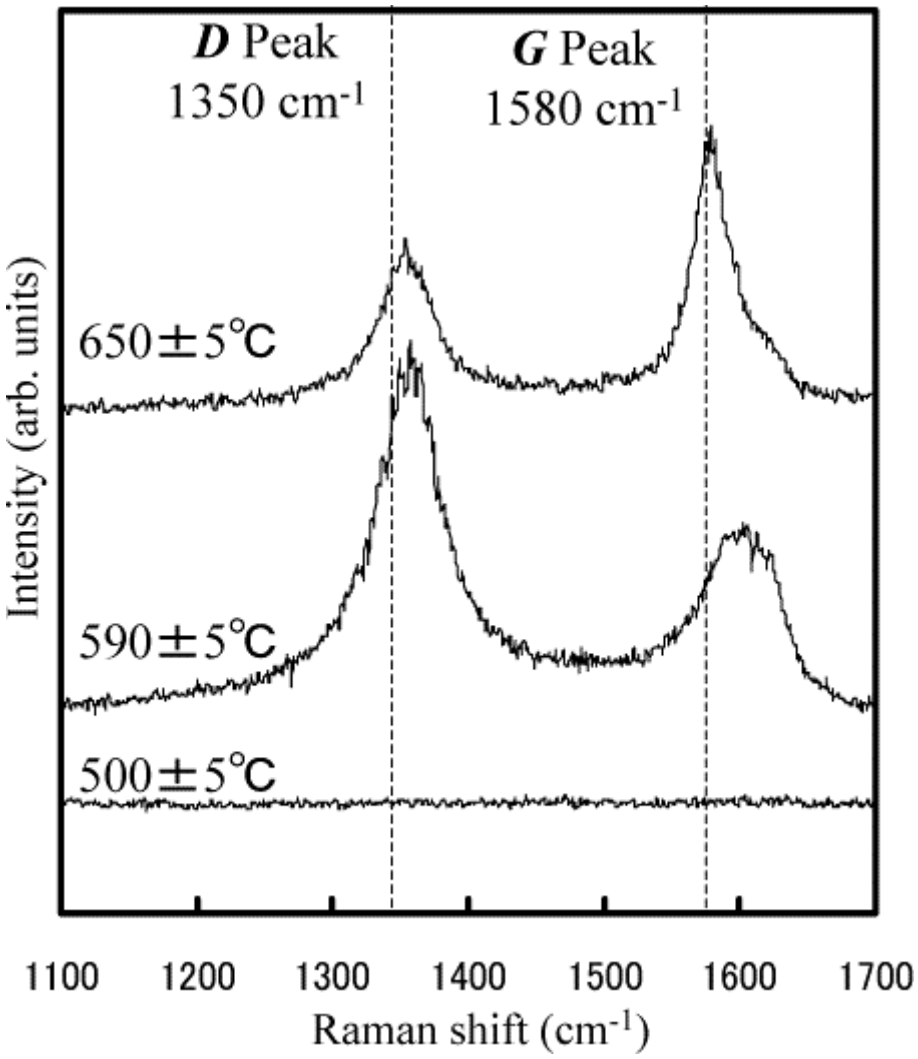

Figure 5.3.1 Ar+ laser Raman spectra

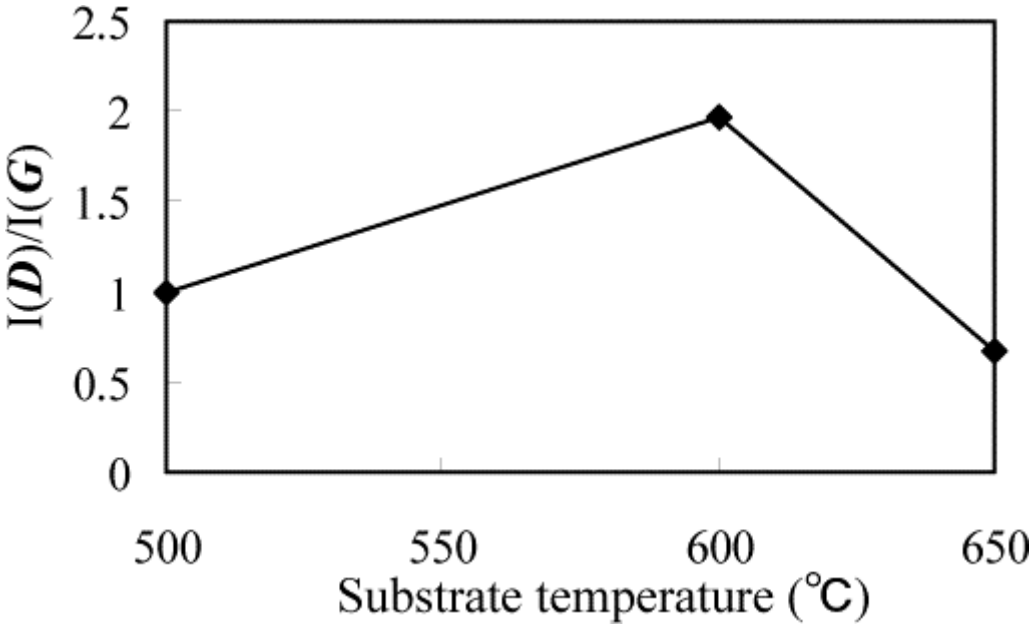

Figure 5.3.2 Ration of D peak against G peak (I(D)/I(G)

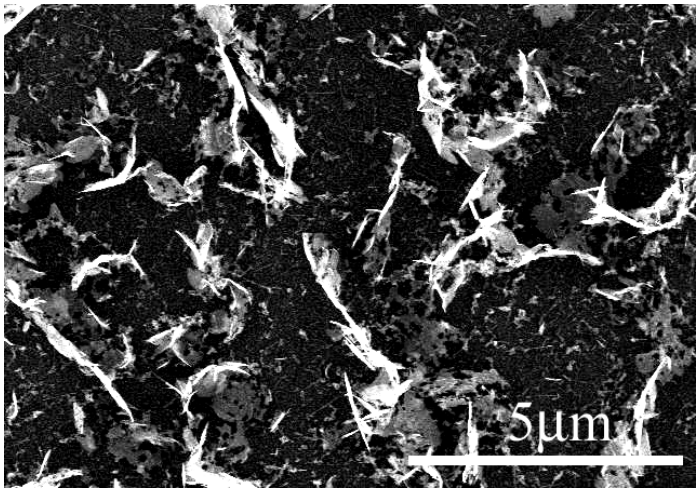

(a) Substrate temperature of 650±5℃

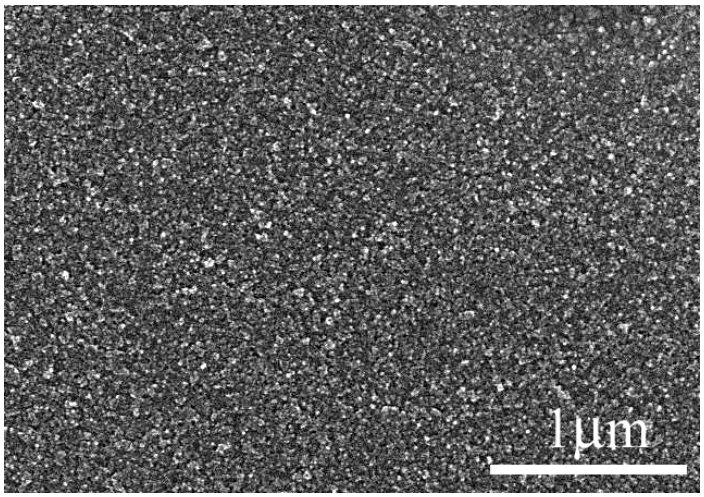

(b) Substrate temperature of 590±5℃

Figure 5.3.3 FE-SEM images

5.4. Characteristics of carbon films deposited at different CO gas concentrates

Using RDL-SWP apparatus, carbon films were synthesized under the conditions of different CO gas concentrations from 3% to 5% with applying –100V DC bias voltages to the upper metal plate.

As the substrate for deposition, n-type mirror-polished silicon (100) was used. The substrates were just cleaned in methanol vessel without any pre-treatment for the nucleation of diamond, and placed on the substrate holder (heater) grounded electrically. And as source gas, gas mixtures of 97%H_2–3%CO, 96%H_2–4%CO, and 95%H_2–5%CO were injected to the discharging chamber. And the gas pressure was preserved as 30±2 mTorr. The incident microwave power was preserved at 1.49 ±0.01kW. The substrate temperatures were controlled as 590±5℃. The characteristics of these synthesized films were analyzed by Ar+ laser Raman spectroscopy.

The experimental conditions are shown in table 5.4.1

Table 5.4.1 Experimental conditions

NO.	DC Bias voltage (V)	Source gas (%)		Duration (hour)
		H2	CO	
1	–100V	97	3	7
2	–100V	96	4	7.8
3	–100V	95	5	7.8

The Ar+ laser Raman spectra of the deposited films is shown in figure 5.4.1. The *D* peaks and *G* peaks are also presented at 1350cm^{-1} and 1580cm^{-1}, respectively. The intensities of the two peaks are increased with increasing the CO concentration.

And the ratio of the intensities of *D* peaks and the intensities of *G* peaks was calculated and plotted in figure 5.4.2. The ratio of I(D)/I(G) is bigger than 2 at every CO gas concentration conditions. This indicates the sp^2 domain and grain size is very small at these all deposition conditions. But increasing the CO gas concentrate, sp^2 sites are generated much more.

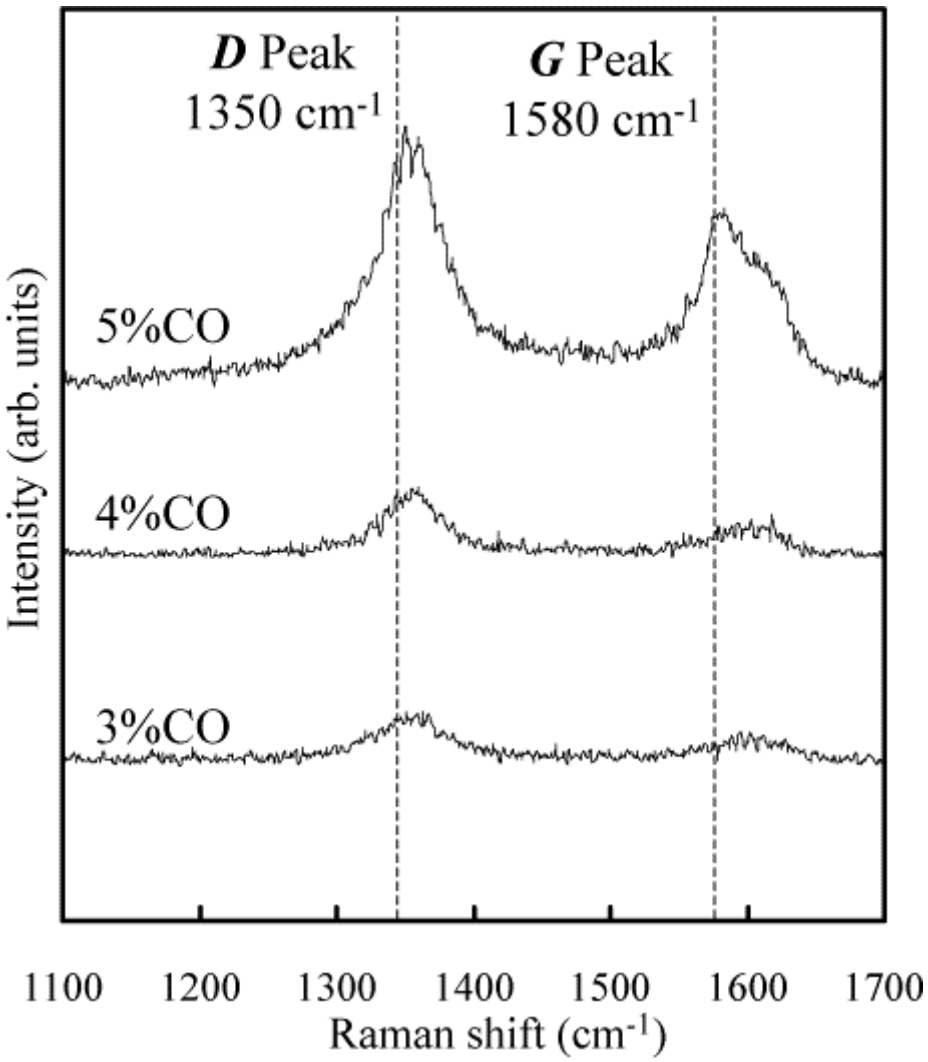

Figure 5.4.1 Ar+ laser spectra

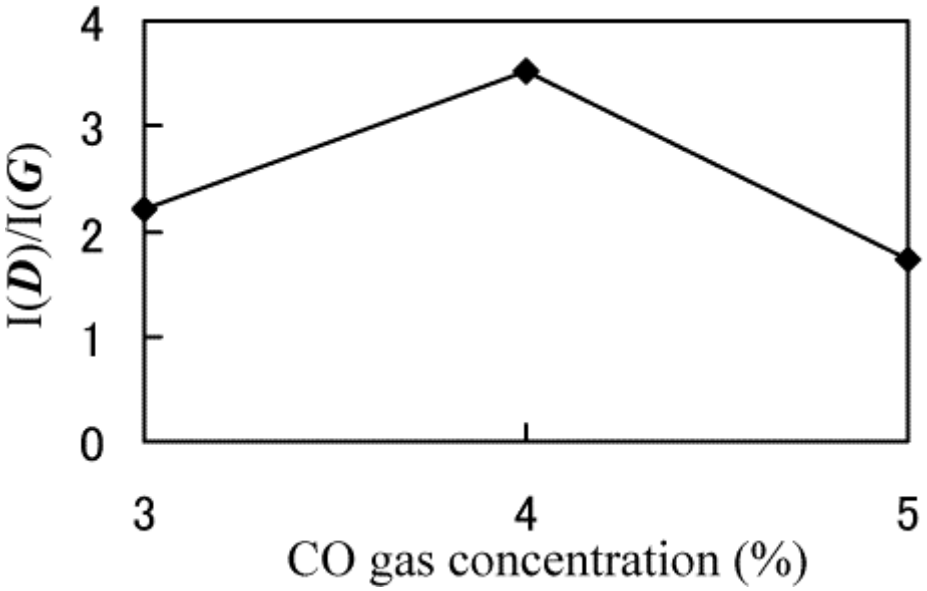

Figure 5.4.2 Ration of D peak against G peak (I(D)/I(G))

6. Conclusion

In this thesis, carbon films were synthesized with applying negative DC bias voltages in RDL-SWP apparatus.

In chapter 2, the negative DC bias method was analyzed theoretically with a simplified plasma model in RDL-SWP plasma. The plasma parameters such as electron temperature, electron density, and space potential in bulk plasma were represented with the plasma parameters in SWP generated region and ratio of surface areas of both electrodes.

In chapter 4, the plasma parameters were measured using the single probe method. The space potential of bulk plasma that occurred CVD process was decreased with increasing the negative DC bias voltage. However, with the saturation of the net current flowing through the electrodes, the space potential was saturated ~11V. Other hand, the electron temperature was decreased linearly against increasing the negative DC bias voltage. And the electron density was increased, although the space potential in bulk plasma was saturated.

In chapter 5, carbon films were synthesized at a low gas pressure of 30mTorr and the conditions of different negative bias voltages, different substrate temperatures, and different CO gas concentrations in RDL-SWP apparatus. On the basis of the measurement results of deposited films, the changing of deposited film morphologies can be plotted as in figure 6.1.1. Moreover, the dependences of DC bias voltages, substrate temperatures, and CO gas concentrations can be described as in figure 6.1.1. However, the detailed physics and relationships with plasma parameters should be studied.

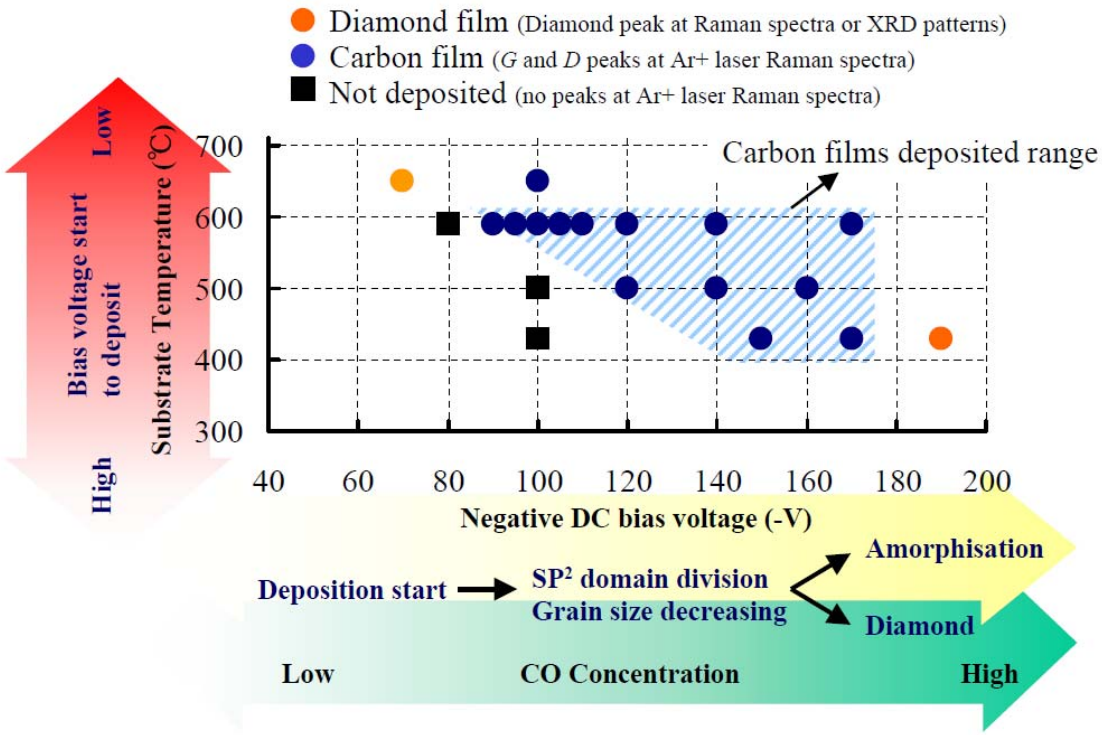

Figure 5.4.1 Dependences on bias voltages, substrate temperatures, and CO gas concentrations

Reference

[1] M.A.Lieberman and A.J.Lichtenberg, “Principles of Plasma Discharges and Materials Processing”, 2nd Edition, John Wiley & Sons Inc. (1994).

[2] G. Bonizzoni, E. Vassallo, “Plasma physics and technology; industrial applications”, Vacuum, Vol. 64, p.327 (2002)

[3] H.Cornads and M.Schmidt, “Plasma generation and plasma sources”, Plasma Sources Sci.Technol., Vol.9, p.441 (2000)

[4] A.Bogaerts, E.Neyts, R.Gijbels, and J.Mullen, “Review: Gas discharge plasmas and their applications”, Elsevier Science B.V., Spectrochimica Acta Part B, Vol.57, p.609 (2002).

[5] R. Bosisio, C. Weissfloch, and M. Wertheimer, “The large volume microwave plasma generator”, J. Microwave Power, Vol.7, p.325 (1972).

[6] A. Maradudin, and D. Mills, “Scattering and absorption of electromagnetic radiation by a semi-infinite medium in the presence of surface roughness”, Phys. Rev. B, Vol.11, p.1392 (1975)

[7] T. Toba, Ph.D. Thesis, The university of Tokyo (2003) (in Japanese).

[8] A.W.Trivelpiece and R.W.Gould, “Space Charge Waves in Cylindrical Plasma Columns”, J. Appl. Phys., Vol.30, No.11, p.1784 (1959).

[9] M.Moisan, Z.Zakrzewski, and R.Pantel, “The theory and characteristics of an efficient surface wave launcher (surfatron) producing long plasma columns”, J. Phys.D: Appl. Phys., Vol.12, No.2, p.219 (1979).

[10] M. Moisan, Z. Zakrzewski, R. Pantel, and P. Leprince, “Waveguide-based launcher to sustain long plasma columns through the propagation of an electromagnetic surface wave”, IEEE Trans. Plasma Sci., Vol.12, No.3, p.203 (1984)

[11] M. Moisan, Z. Zakrzewski, “New surface wave launchers for sustaining plasma columns at submicrowave frequencies (1~300 MHz)”, Rev. Sci. Instrum., Vol.58, p.1895 (1987)

[12] I. Zhelyazkov, and E. Benova, “Modeling of a plasma column produced and sustained by a traveling electromagnetic surface wave”, J. Appl. Phys., Vol.66, p.1641 (1989)

[13] E. Benova, and I. Zhelyazkov, “Theoretical study of the influence of a metal enclosure on the parameters of a plasma column sustained by a traveling electromagnetic surface wave”, Phys. Scr., Vol.43, p.68 (1991)

[14] J. Margot-Chaker, M. Moisan, M. Chaker, V. M. M. Glaude, P. Lauque, J. Paraszczak, and G. Sauvé, “Tube diameter and wave frequency limitations when using the electro magnetic surface wave in the m=1 (dipolar) mode to sustain a plasma column”, J. Appl. Phys., Vol.66, p.4134 (1989)

[15] I. Pérès, M. Fortin, and J. Margot, “The radial structure of a magnetically confined surface-wave plasma column”, Phys. Plasmas, Vol.3, p.1754 (1996)

[16] M.Moisan and Z.Zakrzewski, “REVIEW ARTICLE: Plasma sources based on the propagation of electromagnetic surface waves”, J. Phys.D, Appl. Phys., Vol.24, No.7, p.1025 (1991).

[17] K.Komachi and S.Kobayashi, “Generation of a microwave plasma using traveling waves”, J. Microwave Power and Electromagnetic Energy, Vol.24, No.3, p.140 (1989).

[18] Y.M.Aliev, H.Schluter, and A.Shivarova, “Guided-Wave-Produced Plasmas”, Springer-Verlag, (2000).

[19] W.P.Allis, S.J.Buchsbaum, and A.Bers, “Waves in Anisotropic Plasmas”, M.I.T. press, Cambridge, Massachusetts (1963).

[20] H.Sugai, I.Ghanashev, and M.Nagatsu, “High-density flat plasma production based on surface waves”, Plasma Sources Sci. Technol, Vol.7, No.2, p.192 (1998).

[21] Jaeho Kim, “High Quality Diamond Film Deposition with Surface-Wave Excited Low Pressure Plasma Process Device”, Ph.D. Thesis, The university of Tokyo (2003).

[22] Collin R. E., “Field Theory of Guided Waves”, New york , McGraw-Hill

[23] F.Werner, D.Korzec, and J.Engemann, “Slot antenna 2.45GHz microwave plasma source” Plasma Sources Sci. Technol., Vol.3, No.4, p.473 (1994).

[24] M.Nagatsu, G.Xu, I.Ghanashev, M.Kanoh, and H.Sugai, “Mode identification of surface waves excited in a planar microwave discharge”, Plasma Sources Sci. Technol., Vol.6, p.427 (1997).

[25] M.Kanoh, K.Aoki, T.Yamauchi, and Y.Kataoka, “Microwave-Excited Large-Area Plasma Source Using a Slot Antenna”, Jpn. J. Appl. Phys., Vol.39, Part 1, No.9A, p.5292 (2000).

[26] K.Komachi, “Affecting factors on surface-wave-produced plasma”, J.Vac.Sci. Technol.A, Vol.11, No.1, p.164 (1993).

[27] J. Robertson, “Diamond-like amorphous carbon”, Mater. Sci. and Engineering R, Vol.37, p.129 (2002)

[28] T.Sharda and S.Bhattacharyya, “Encyclopedia of Nanoscience and Nanotechnology”, Vol.2, p.337 (2004)

[29] A. Mitura, K. Mitura, P. Niedzielski, P Louda, and V. Danilenko, “Nanocrystalline diamond, its synthesis,properties and applications”, J. Achivement Mater. Manufacturing Engineering, Vol. 16, No.1-2, p.9 (2006).

[30] C. Popov, W. Kulisch, M. Jelinek, A.Bock, and J. Strnad, “Nanocrystalline diamond/ amorphous carbon composite films for applications in tribology, optics and biomedicine”, Thin Solid Films, p.92 (2006).

[31] F.J. Hernandez Guillen, K. Janischowsky, W. Ebert, and E. Kohn, “Nanocrystalline diamond films for mechanical applications”, phys. Stat. Sol (a), Vol.201, No.11, p.2553 (2004).

[32] K.Teii, and T.Yoshida, “Lower pressure limit of diamond growth in inductively coupled plasma”, J. Appl. Phys., Vol.85, No.3, p.1864 (1999).

[33] Kungen Teii, Tomohiro Ikeda, Atsushi Fukutomi, and Kiichiro Uchino, “Effect of hydrogen plasma exposure on the amount of trans-polyacetylene in nanocrystalline diamond films”, J.Vac. Sci. Technol. B, Vol.24, No.1 (2006)

[34] J. Kim and M. Katsurai, “Control of plasma space potentials and chemical vapor deposition of nanocrystalline diamond films in surface-wave excited low-pressure plasmas”, J. Appl. Phys., Vol.101, p.023301 (2007).

Publication List

Conference

D. Kim, and H. Ohsaki, “Synthesis of Nano-crystalline Diamond Using Surface Wave Plasma Apparatus”, The 8th University of Tokyo - Seoul National University Joint Seminar on Electric Engineering, (Feb 2007)

D. Kim, and H. Ohsaki, “Deposition of Carbon Films with Controlling the Plasma Space Potential of Surface Wave exited Plasma”, The 68th Autumn meeting, The Japan Society of Applied Physics, (Sep 2007)

D. Kim, and H. Ohsaki, “Influences of Plasma Space Potential and Substrate Temperature on Nanocrystalline Diamond Film Deposition in Surface Wave Plasma Apparatus”, The 18th MRS-J Symposium, (Oct 2007)

D. Kim, and H. Ohsaki, and K. Makoto, “Synthesis of Nanocrystalline Diamond Films using Surface Wave exited Plasma CVD Apparatus”, The Papers of Technical Meeting on Plasma Science and Technology, IEE Japan, (Dec 2007)

D. Kim, H. Ohsaki, and K. Makoto, “Influence of Substrate Temperature on Carbon Film Deposition in Surface Wave exited Plasma CVD Apparatus”, National Convention IEE Japan, (Mar 2008) (Planed)

Others

Paper

M. Sekino, D. Kim, and H. Ohsaki, “FDTD simulations of RF electromagnetic fields and signal inhomogeneities in ultrahigh-field MRI systems”, Journal of Applied Physics (in press).

Conference

M. Sekino, D. Kim, S. Ueno, and H. Ohsaki, “RF Absorption in The Human Head in a 11.7T MRI System”, National Convention IEE Japan, (Mar 2007)

M. Sekino, D. Kim, S. Ueno, and H. Ohsaki, “RF absorption in the human head in ultrahigh-field magnetic resonance imaging systems of up to 11.7 T”, 29th Annual Meeting of the Bioelectromagnetics Society, Kanazawa, Japan, (Jun 2007).

D. Kim, M. Sekino, S. Ueno, and H. Ohsaki, “Numerical Simulations of High-Frequency Elecromagnetic Fields inUltra high-Magnetic-Field MRI Systems”, Mag-07-79, (Sep 2007)

M. Sekino, D. Kim, and H. Ohsaki, “FDTD simulations of RF magnetic fields and signal inhomogeneities in high-field MRI systems”, 52nd Magnetism and Magnetic Materials Conference, Tampa, USA, (Nov 2007).

J. Kim, K. Makoto, D. Kim, and H. Ohsaki, “Discharging characteristics of microwave excited blowing-type atmospheric-pressure plasmas using microstrip-line technology”, The Papers of Technical Meeting on Plasma Science and Technology, IEE Japan, (Dec 2007)

Patent

Atmosphere Blowing typed Plasma Device, Jaeho Kim, Dongmin Kim, Hiroyuki Ohsaki, Katsurai Makoto, (May 2007)

Acknowledgments

Many people have contributed to this study directly or indirectly. I would like to express my gratitude to all of them.

First of all, I would like to thank my supervisor Prof. Hiroyuki Ohsaki for his support and advice. Although my slow progress, you have always waited for me with patience.

And I would like to thank Prof. Makoto Katsurai for his scientific discussions and advices. I also highly appreciate the helpful advices and supports of Jaeho Kim. I have learned many things about not only plasma but also life from you.

I am extremely grateful to the members of our Ohsaki lab. I thank Dr. Masaki Sekino for his scientific advices. And I am very grateful to Yasuhito Ueda, Satoshi Tatara, Tatsuya Suzuki, Yoshiki Komi, Souhei Nonaka, Sinji Wasada, and Yuko Yamazaki.

Further, I would like to thank Prof. Kazuo Terashima and members of his lab for share me XRD and SEM devices. I am also highly grateful to Prof. Motoichi Ohtsu and members of his lab for support to use FE-SEM. I would like to express also my gratitude to Dr. Akio Susa for share me Ar+ laser Raman spectroscopy.

Finally, I would like to thank my parents, my sister, and my wife for their kindness, patience, support, and encouragement. I really thank you.